IONO THREAT ANALYSIS IN CANARY ISLANDS

AMENICA3

Prepared by: Alberto de la Fuente

Approved by: Alberto de la Fuente

Authorized by: Alberto de la Fuente

Code:	GMV-AMENICA3-DEL-001
Version:	v2.1
Date:	25/11/2016
Internal code:	GMV 22237/16 V3/16

GMV AEROSPACE AND DEFENCE S.A.
Isaac Newton, 11; PTM Tres Cantos; Madrid 28760
Tel. +34 918072100; Fax. +34 918072199
www.gmv.com

DOCUMENT STATUS SHEET

Version	Date	Pages	Changes
v1.0	12/07/2016	30	First version delivered.
v2.0	16/09/2016	36	Results after analysing 20 additional periods (Set 2).
v2.1	25/11/2016	42	Update the document after the review of ENAIRE.

TABLE OF CONTENTS

LIST OF TABLES AND FIGURES

1. INTRODUCTION

1.1. PURPOSE

The purpose of this document is to analyse the ionospheric spatial gradients occurred in the Canary Islands from January 2009 to December 2015 (solar cycle 24th). The analyses of these gradients and its comparison with the ionospheric threat model of GBAS GAST-C stations, is a key element to evaluate the integrity of these stations.

1.2. SCOPE

This document has been delivered by GMV in the frame of AMENICA3 project for ENAIRE [AD.1].

1.3. DEFINITIONS AND ACRONYMS

1.3.1. DEFINITIONS

Concepts and terms used in this document and needing a definition are included in the following table:

Table 1-1 Definitions

Concept / Term	Definition
Single-SV	Compute gradients pairing up IPPs belonging to the same SV
Crossing time delay	Time elapsed when the ionospheric front passes over two receivers.
Slant Delay (STEC)	Ionospheric delay computed along the line of sight.
Vertical Delay (VTEC)	Ionospheric slant delay modified with a 'mapping function' to remove any dependency with the elevation of the line of sight.

1.3.2. ACRONYMS

Acronyms used in this document and needing a definition are included in the following table:

Table 1-2 Acronyms

Acronym	Definition
AD	Applicable Document
AS	Anti-Spoofing
CAT-I	Category I
CONUS	CONtiguous United States
EPN	EUREF Permanent Network
ETRS89	European Terrestrial Reference System 89
GBAS	Ground Based Augmentation System
GPS	Global Positioning System
IEA	Ionospheric Equatorial Anomaly
IGN	Instituto Geográfico Nacional
IGS	International GNSS Service
IGWG	International GBAS Working Group
IPP	Ionospheric Pierce Point
GNSS	Global Navigation Satellite System
LAAS	Local Area Augmentation System
LOS	Line Of Sight
RD	Reference Document
RINEX	Receiver INdependent EXchange Format

Acronym	Definition
SBAS	Satellite Based Augmentation System
SC	Solar Cycle
SID	Sudden Ionospheric Disturbances
STEC	Slant TEC
TEC	Total Electron Content
VTEC	Vertical TEC

2. REFERENCES

2.1. APPLICABLE DOCUMENTS

The following documents, of the exact issue shown, form part of this document to the extent specified herein. Applicable documents are those referenced in the Contract or approved by the Approval Authority. They are referenced in this document in the form [AD.X]:

Table 2-1 Applicable documents

Ref.	Title	Code	Version	Date
[AD.1]	Proposal for AMENICA3	GMV 12185/15 V4/15		15/10/2015

2.2. REFERENCE DOCUMENTS

The following documents, although not part of this document, amplify or clarify its contents. Reference documents are those not applicable and referenced within this document. They are referenced in this document in the form [RD.X]:

Table 2-2 Reference documents

Ref.	Title	Code	Version	Date
[RD 1]	Iono Threat Analysis In Canary Islands GMV 20360/15 V3/15	GMV-AMENICA2-DEL-001	1.2	10/04/2015

3. METHODOLOGY

3.1. PURPOSE

The ionospheric threat analysis intends to obtain a general view of the ionosphere behaviour considering only ionosphere high-activity events. These events, which lead to very high spatial gradients (i.e. difference of ionospheric delay between two IPPs divided by the separation distance between both IPPs), are the scope of this analysis.

The ionosphere high-activity events are typically: ionospheric storms, ionospheric equatorial anomaly (IEA) or bubbles. These events are modelled as a linear front moving at a constant speed, being the front parameterized by the spatial gradient.

3.2. SINGLE SV CONCEPT

Honeywell's methodology for ionospheric storm evaluation is based on the Stanford threat model and makes use of the '*single-SV*' concept, which consists in computing gradients from a pair of stations between lines-of-sight (LOS) of the same satellite. This requires a dense cluster of stations, where the stations are close enough (e.g. typically less than 50km).

This technique makes LOS almost parallel and, thus, distance between IPPs is almost constant and approximately equal to the baseline distance between stations. Provided a high density grid of receivers, this procedure has following advantages:

- Higher probability to detect the largest gradient of the ionospheric event.
- Ionosphere thin-shell model has no effects because LOS are parallel and close.
- No need to estimate Inter-frequency bias (IFB) of the SVs, because they are automatically removed when differencing ionospheric delays of IPPs belonging to the same SV.
- No need to screen the elevation and azimuth of each IPP as they are parallel.

Note. In the analysis described in this document, gradients are computed as 'vertical' delays (VTEC) and they are mapped to 'slant' delays (STEC) using the mapping function. The reason is that the model (Figure 7-1) uses STEC.

An outline of the '*single-sv*' concept is shown below.

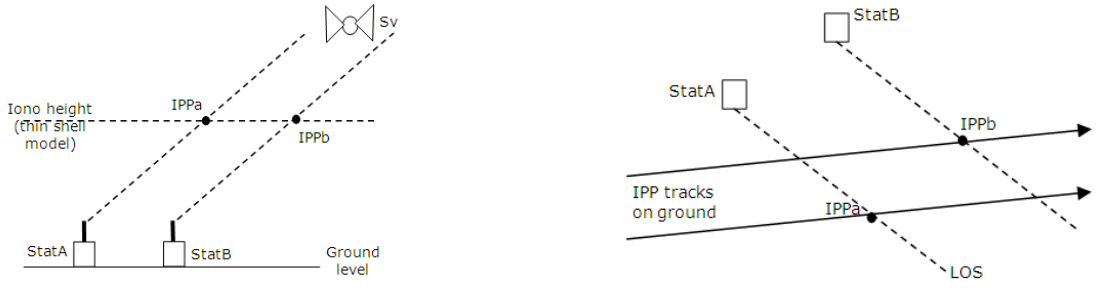

Elevation drawing

Ground-plan drawing

Figure 3-1 'Single SV' concept

3.3. ANALYSIS

This section describes the process followed to analyse of the ionospheric storm evaluation. The analysis has following steps:

1. **Identify days.**

   For mid-geomagnetic latitudes, days suspicious to have large gradients are highly correlated with space weather parameters (Kp, Dst and AE). To avoid analysing all the days, *suspicious* days are selected with module "StormyDaysIdentification".

However, for low-geomagnetic latitudes there is not such large correlation, and bubbles or enhanced IEA might be observed whereas space weather parameters remain at normal levels. For this reason, the ionosphere threat analyses for low-geomagnetic latitudes shall analyse all the days (not only the *suspicious* days).

The analysis described in this document covers the Canary Islands, which is considered "low-latitude" in terms of ionospheric activity, and therefore it requires the analysis of all the days. In order to reduce the amount of data to process, only days that have been already identified by Eurocontrol, will be analysed. See §5.

Note. Eurocontrol, in the frame of GIMA project and SESAR 15.3.4, has analysed the ionosphere activity for all days in ECAC area.

2. **Evaluate "storms".**

   Automatic processing to compute ionospheric delay using double frequency L1/L2 GPS raw phase. P1/P2 GPS raw code is used to remove ambiguity.

   In addition, IFB of the stations is estimated for each day.

   RINEX 1Hz data is used.

   Once the ionospheric delays and the IFBs are obtained, the largest ionospheric gradients are computed using 'single-SV' concept.

3. **Manual confirmation of gradients.**

   Human evaluation to reject gradients generated by other artefacts than ionosphere (e.g. multipath).

   Finally, the results of this analysis (i.e. largest gradients confirmed) are shown in §6.

The software modules used to obtain the ionosphere delay slope estimations have been inherited from the first project AMENICA, and they have been updated to process input RINEX at 1Hz. These modules are:

- StormyDaysIdentification.
- GetRINEXData.
- DataProcessing.
- IonoDelaySlopeComputation.
- GetHighSlopes.
- GradientConfirmation.
- GetTrueGradients.

Figure 3-2 shows the sequence to run the software modules to ionospheric spatial gradients.

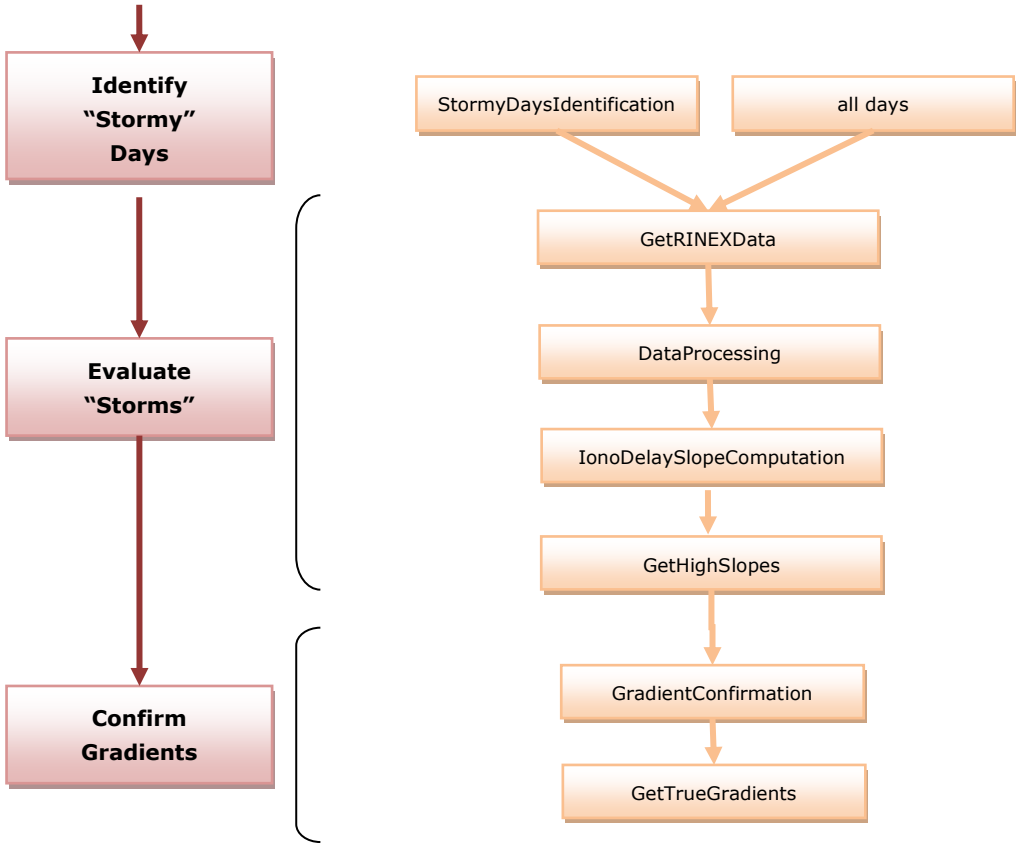

Figure 3-2 Steps for the execution

4. NETWORK OF STATIONS

Since the analysis is to be done in the Canary Islands region, a cluster of stations at or near the islands must be used. Each station belongs to the networks detailed in the tables below.

These networks shall allow access to the RINEX observation files through FTP.

Note. Raw observations at 30s are typically available through FTP. On the other side, raw observations at 1s are only available in FTP from the last 6 months. For this reason, 1s RINEX files were requested to the entities managing the networks.

In the analysis described in this document the networks used are: IGS, IGN, and GRAFCAN. Table 4-1 shows the list of stations used for the analysis in the Canary Islands territory or in the vicinity.

Table 4-1 GPS receivers used in the Canary Islands

Station ID	Network	# Stations
mas1, pdel	IGS	2
tn01, tn02, tn03, fuer, lpal, izan	IGN	6
tias, yaiz, anti, agui, alde, graf, snmg, alaj, fron, hria, oliv, tara, morj, argu, terr, stei, mazo	GRAFCAN	17

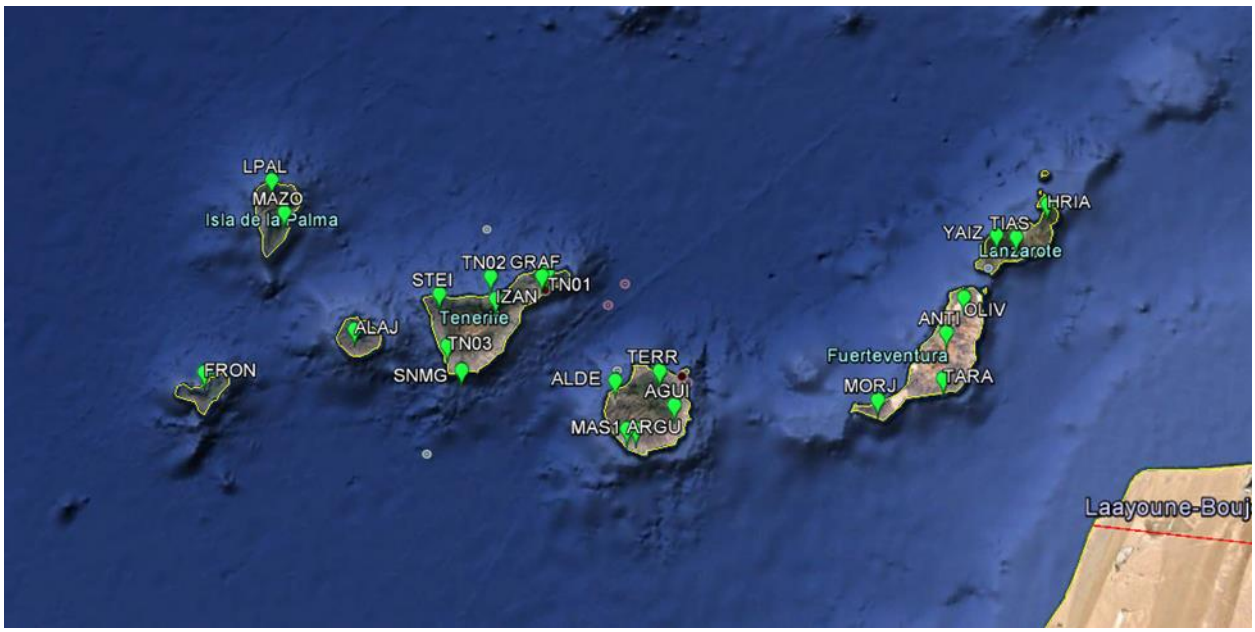

Figure 4-1. Location of the stations used in the analyses. (Courtesy by Google Earth)

Table 4-2 lists the stations used in the calculation but too far from the territory of interest to be taken into consideration for the analysis. These stations are added to improve the estimation of the stations hardware biases.

Table 4-2 GPS receivers far from the Canary Islands

Station ID	Network	# Stations
gold, tidb, suth, kour	IGS	4

The observation data available for the stations of each network has been extracted from the FTPs listed in Table 4-3.

RINEX observation files at 1Hz are only available in ftp server of IGN and GRAFCAN for the latest 6 months. For this reason, it is appreciated that **IGN and GRAFCAN provided a full-set of RINEX at 1Hz**.

Table 4-3 FTP addresses used for each network

Network	FTP data
IGS	ftp://cddis.gsfc.nasa.gov
IGN	N/A
GRAFCAN	N/A

5. DAYS SELECTED

This section lists the days of the current solar cycle 24th maximum (January 2009 to December 2015) that have been analysed in this study.

As detailed in §3.3 the first step of the process is to detect those days suspicious to have high ionospheric activity. Considering that Canary Island belongs to low-geomagnetic latitude, using geomagnetic indices to identify these days might not be enough. For this reason, days identified by Eurocontrol in its ionosphere analyses have been selected.

Tables below show the **35 days** with large spatial ionospheric gradients, according to the **results of Eurocontrol**.

Note. Set 1 contains the days with higher gradients than days in Set 2, according to Eurocontrol's results. Days of Set 1 were analysed in the first version of the document, whereas days of Set 2 were added in the version 2.0 of the document.

Table 5-1 Days Identified. Set 1

Period Id	Year	Month	Day	Source
25	2012	10	16	Eurocontrol
32	2013	10	16	Eurocontrol
33	2013	10	17	Eurocontrol
34	2013	10	22	Eurocontrol
35	2013	12	31	Eurocontrol
42	2014	03	17	Eurocontrol
43	2014	03	31	Eurocontrol
47	2014	04	08	Eurocontrol

Period Id	Year	Month	Day	Source
51	2014	09	13	Eurocontrol
53	2014	09	27	Eurocontrol
54	2014	09	30	Eurocontrol
55	2014	10	05	Eurocontrol
56	2014	10	06	Eurocontrol
64	2015	02	06	Eurocontrol
65	2015	02	19	Eurocontrol

Table 5-2 Days Identified. Set 2

Period Id	Year	Month	Day	Source
24	2012	10	15	Eurocontrol
31	2013	10	06	Eurocontrol
36	2014	01	20	Eurocontrol
38	2014	03	01	Eurocontrol
39	2014	03	03	Eurocontrol
40	2014	03	09	Eurocontrol
44	2014	04	02	Eurocontrol
45	2014	04	03	Eurocontrol
46	2014	04	06	Eurocontrol
48	2014	04	11	Eurocontrol

Period Id	Year	Month	Day	Source
49	2014	09	03	Eurocontrol
52	2014	09	20	Eurocontrol
57	2014	10	09	Eurocontrol
58	2014	11	11	Eurocontrol
59	2014	11	22	Eurocontrol
60	2014	12	01	Eurocontrol
61	2014	12	15	Eurocontrol
62	2014	12	23	Eurocontrol
66	2015	03	06	Eurocontrol
71	2015	04	23	Eurocontrol

Following figures shows the number of stations available in these periods is enough to obtain reliable results. In all periods there were more than 23 stations in the Canary Islands cluster.

In addition, it is confirmed that these days reflect high ionosphere activity because the number of cycle-slips is very high for the station located in Canary Islands (e.g. mas1) but not for the other stations (e.g. gold). See Figure 5-3 and Figure 5-4.

Note. The number of cycle slips includes not only the cycle slips detected within one arc, but also the new arcs due to data gaps in both frequencies L1/L2. The high ionosphere activity provokes losing tracking (mainly in L2) and therefore data gaps.

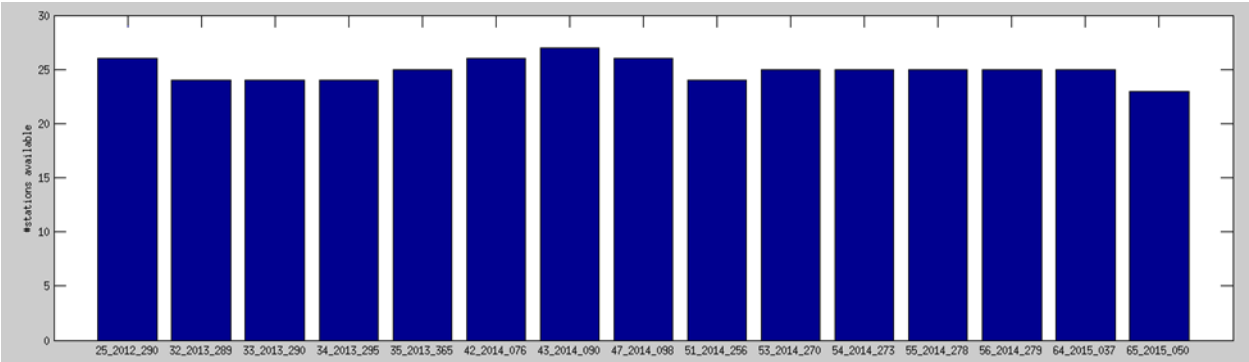

Figure 5-1. #Stations available per period. Set 1

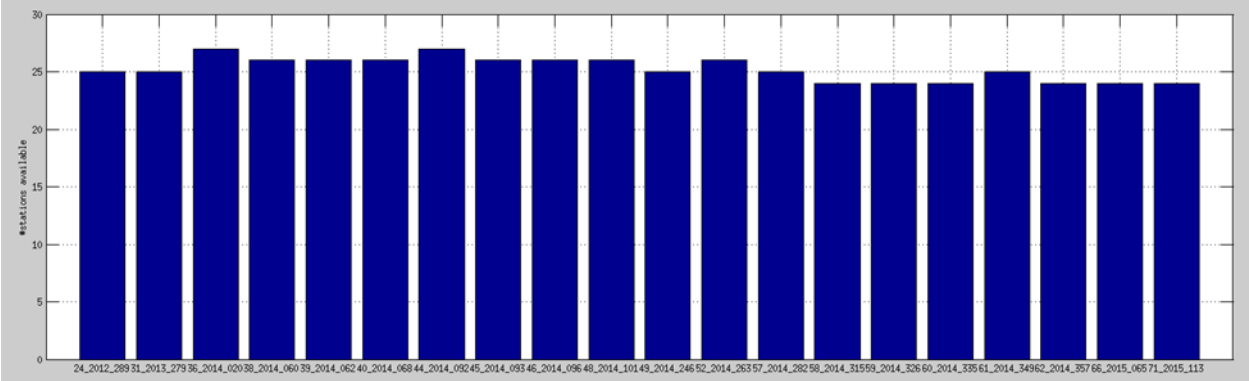

Figure 5-2. #Stations available per period. Set 2

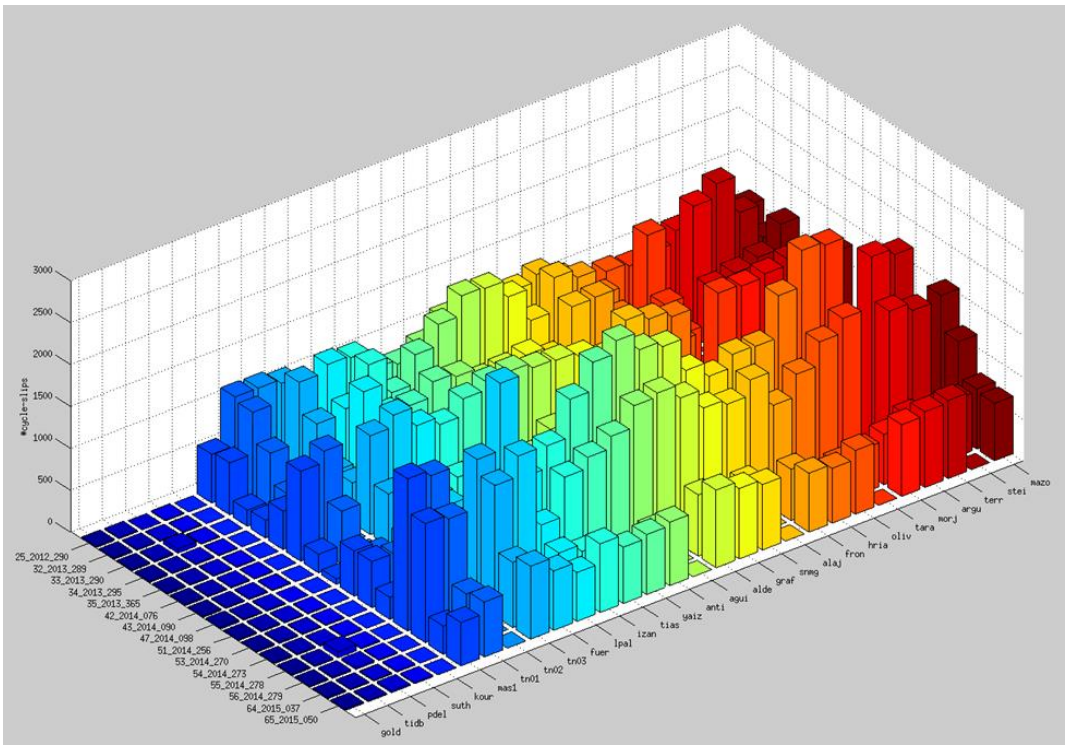

Figure 5-3. #Cycle-Slips per period and per stations. Set 1.

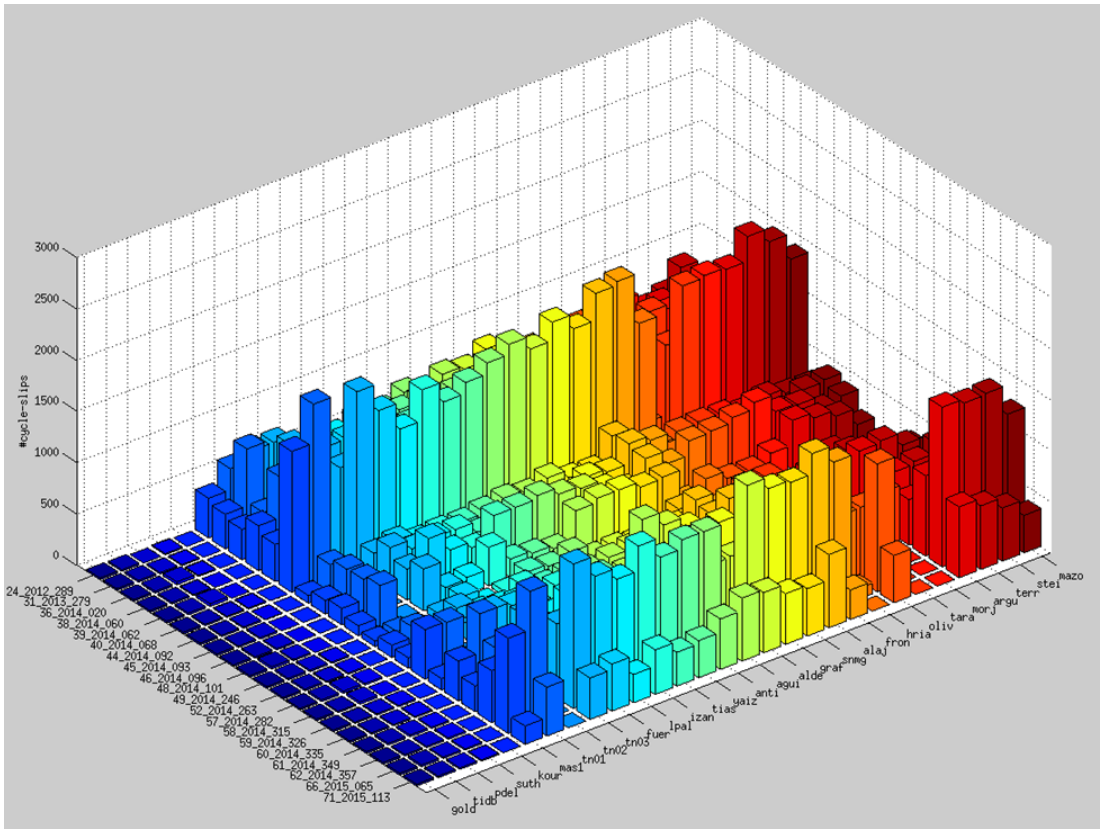

Figure 5-4. #Cycle-Slips per period and per stations. Set 2.

According to the solar cycle progression (see figure below) in terms of sunspot number, the highest ionosphere activity during current solar cycle was reached since 2011 to 2014 (both included).

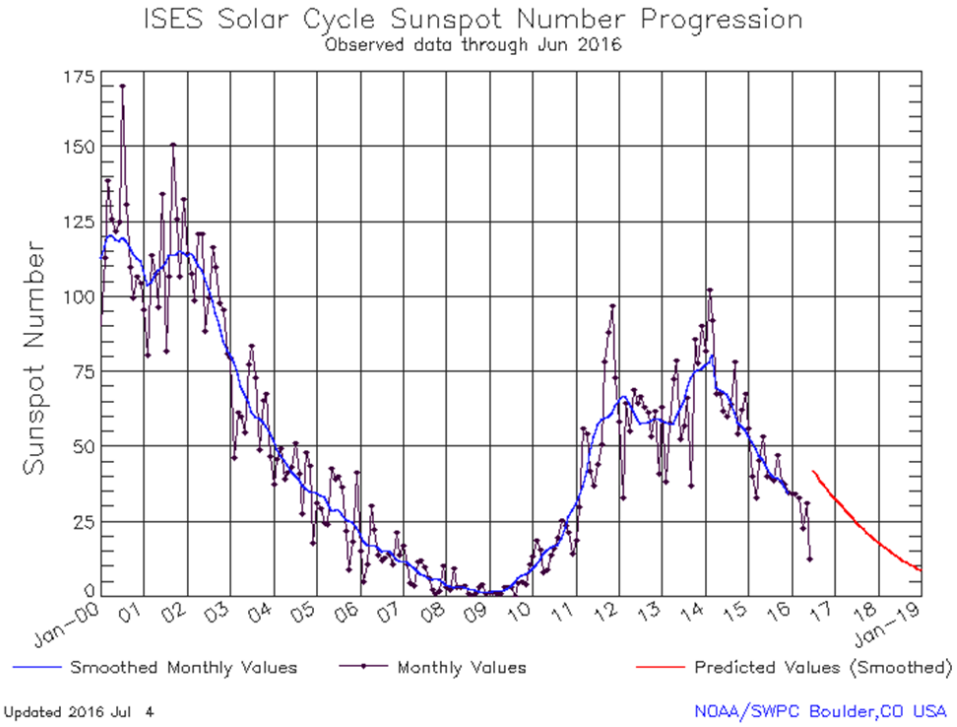

http://www.swpc.noaa.gov/products/solar-cycle-progression

Figure 5-5 Solar cycle progression and forecast (SWPC NOAA)

6. RESULTS

This section describes the largest gradients obtained and confirmed in this analysis, listed in Table 6-1, including following information for each gradient:

- Gradient Id: identification number.
- Set: set 1 or 2 according to §5.
  Note. Gradient Id and Set identify univocally each gradient.
- Period Id and GPS Second: the period where the gradient belongs to (see §5.), and the epoch (GPS Time) when the gradient occurred.
- Station A, Station B and PRN: IPPs where the gradient was detected. Two Stations and one PRN
- Elevation.
- IPP Dist: Distance between the IPP (considering ionosphere thin-shell model with height 350km).
- Gradient VTEC: Ionospheric spatial gradient (VTEC).
- $Grad_{TRUE}$ VTEC: gradient estimated after manual correction. See Annex I.
- $Grad_{TRUE}$ STEC: Ionospheric spatial gradient (STEC) used in the thread model.

In addition, for each periods with large gradients, the corresponding subsection includes these plots:

- Map with the ionospheric delay (VTEC) at the epoch when the gradient occurred.
  White and yellow markers refer to the IPP (diamonds) and the station (squares) of the gradient.
- Time evolution of the ionospheric delay (VTEC) for each IPP and the gradient in vertical mm/km.

Note. Larger gradients were detected in very close stations (IPP distance shorter than 5km). In this case, small errors during the estimation of the stations' hardware bias might provoke large errors in the estimation of the gradients.

Table 6-1. Largest gradients obtained in this analysis.

Gradient Id	Set	Period Id	GPS Second	Station A	Station B	PRN	Elevation [°]	IPP Dist [km]	Gradient VTEC [mm/km]	$Grad_{TRUE}$ VTEC [mm/km]	$Grad_{TRUE}$ STEC [mm/km]
29	**1**	**33**	421814	argu	mas1	9	61.8	4.6	472.9	*330	368.4
~~**31**~~	~~**1**~~	~~**56**[1]~~	~~90504~~	~~argu~~	~~mas1~~	~~12~~	~~27.5~~	~~4.5~~	~~461.8~~	~~*313~~	~~568.3~~
36	**1**	**33**	422763	argu	mas1	8	62.6	4.6	444.0	*341	378.3
87	**1**	**33**	421448	argu	mas1	9	59.1	4.6	360.3	*279	318.7
93	**1**	**51**	602088	argu	mas1	2	62.7	4.6	357.4	*226	250.5
1	1	32	337932	agui	mas1	4	41.2	23	325.2	*255	361.1
9	1	32	337859	alde	terr	4	41.4	23.5	254.4	=	359.1
2	**2**	**40**	80984	anti	fuer	31	77.3	16.9	243.9	=	249.3
5	2	58	252278	snmg	tn03	5	51.2	11.2	238.1	=	294.8
7	**2**	**40**	81230	tias	yaiz	31	79.1	10.6	232.56	=	236.3
13	1	34	251510	snmg	tn03	4	29.5	10.9	228.9	=	398.9
15	**1**	**33**	422192	agui	alde	9	64.2	33.1	225.8	=	247.5
16	1	55	4695	anti	fuer	12	29.0	15.6	225.7	=	397.3
10	2	66	512091	tias	yaiz	31	78.7	10.6	224.6	=	228.5
18	1	34	253242	tias	yaiz	2	43.2	10.4	222.7	=	306.1
19	**1**	**51**	601309	alde	terr	6	46.2	23.6	220.4	=	290.4
20	1	64	438291	tias	yaiz	31	32.9	10.5	219.5	=	358.1

[1] Gradient rejected. See §6.3.

Gradient Id	Set	Period Id	GPS Second	Station A	Station B	PRN	Elevation [°]	IPP Dist [km]	Gradient VTEC [mm/km]	$Grad_{TRUE}$ VTEC [mm/km]	$Grad_{TRUE}$ STEC [mm/km]
13	2	36	166247	snmg	tn03	29	34.5	11.0	216.2	=	342.4
21	**1**	**51**	601395	agui	argu	6	45.8	27	215.7	=	285.8
23	**1**	**56**	90934	snmg	tn03	12	30.8	10.6	212.2	=	360.4
17	2	24	169190	snmg	tn03	2	63.6	11.1	211.5	=	232.9
33	**1**	**24**	421793	snmg	stei	8	56.4	28.3	209.9	=	245.9
20	2	45	426605	agui	mas1	31	47.76	23.1	209.2	=	270.1

Following subsections provide more information of the periods with highest VTEC gradients (marked in bold).

- Period 33. See §6.1
- Period 40. See §6.2
- Period 56. See §6.3
- Period 51. See §6.4

Following subsections provide more information of the periods with highest STEC gradients (not included before). Medium VTEC gradients at low elevations provoke high STEC gradients.

- Period 34. See §6.5
- Period 55. See §6.6

Note. Local time in Canary Islands is equal to UTC+1 during Summer Time (April to October) and UTC during rest of the year.

6.1. PERIOD 33

Table below shows the largest gradients for this period.

Table 6-2 Period 33. Gradients

Gradient Id	Set	GPS Time	UTC Time	Station A	Station B	PRN	Elevation [º]	IPP Dist [km]	$Grad_{TRUE}$ VTEC [mm/km]	$Grad_{TRUE}$ STEC [mm/km]
29	1	421814	21h09:58	argu	mas1	9	61.8	4.6	*330	368.4
36	1	422763	21h25:47	argu	mas1	8	62.6	4.6	*341	378.3
87	1	421448	21h03:52	argu	mas1	9	59.1	4.6	*279	318.7
15	1	422192	21h16:16	agui	alde	9	64.2	33.1	225.8	247.5
24	1	421793	21h09:37	snmg	stei	8	56.4	28.3	209.9	245.9

Gradients detected in this period occurred around 21h (local time), during the sunset.

These gradients are due to enhance IEA, not bubbles. It is confirmed thanks to the temporal evolution of the ionospheric delay shown in §9.

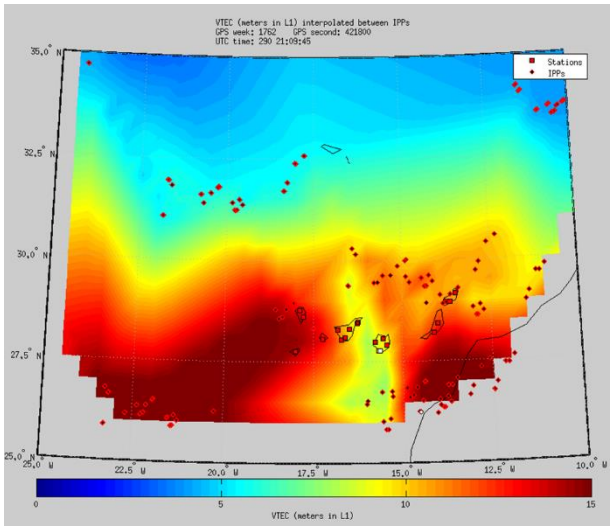

Figure 6-1. Gradient 29 VTEC map.

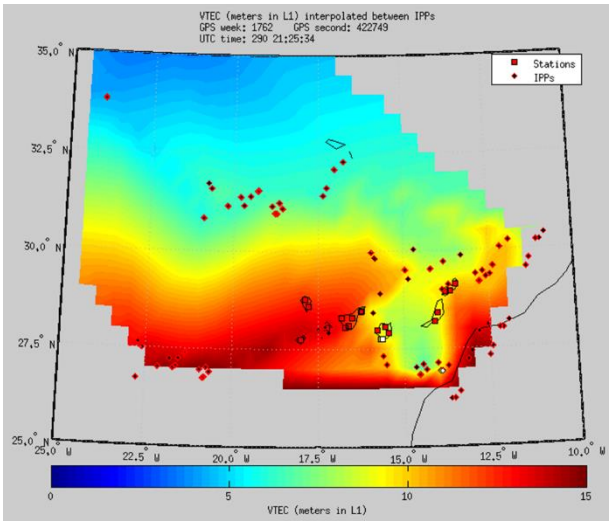

Figure 6-2. Gradient 36 VTEC map.

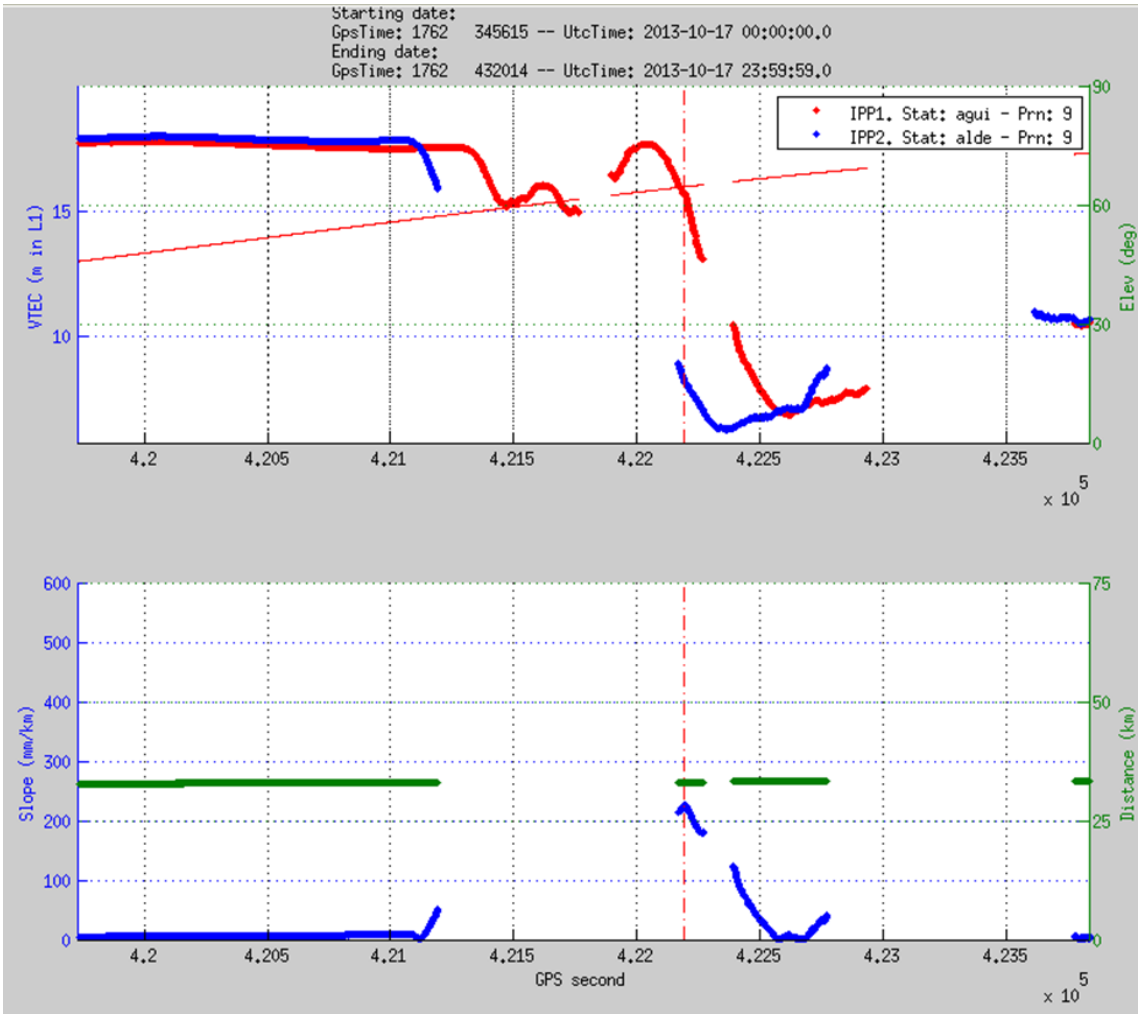

Figure 6-3. Gradient 15. VTEC and gradient.

6.2. PERIOD 40

Table below shows the largest gradients for this period.

Table 6-3 Period 40. Gradients

Gradient Id	Set	GPS Time	UTC Time	Station A	Station B	PRN	Elevation [º]	IPP Dist [km]	$Grad_{TRUE}$ VTEC [mm/km]	$Grad_{TRUE}$ STEC [mm/km]
2	2	80984	22h29:29	anti	fuer	31	77.3	16.9	243.9	249.3
7	2	81230	22h33:35	tias	yaiz	31	79.1	10.6	232.56	236.3

Gradients detected in this period occurred around 22h (local time), during the sunset.

These gradients are due to enhance IEA, not bubbles. It is confirmed thanks to the temporal evolution of the ionospheric delay shown in §9.

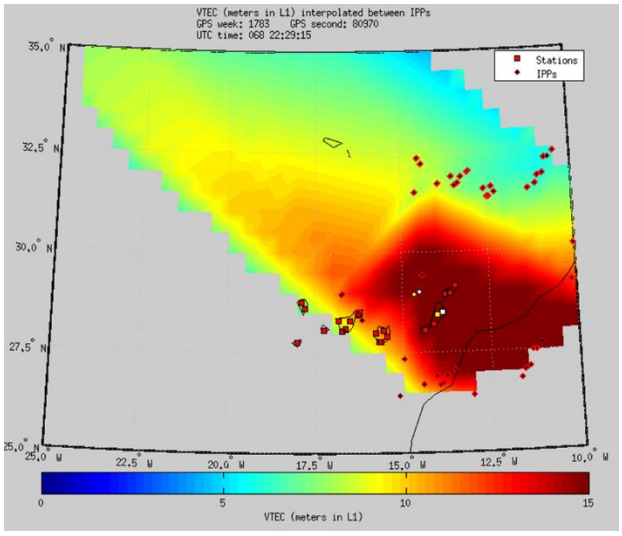

Figure 6-4. Gradient 2 VTEC map.

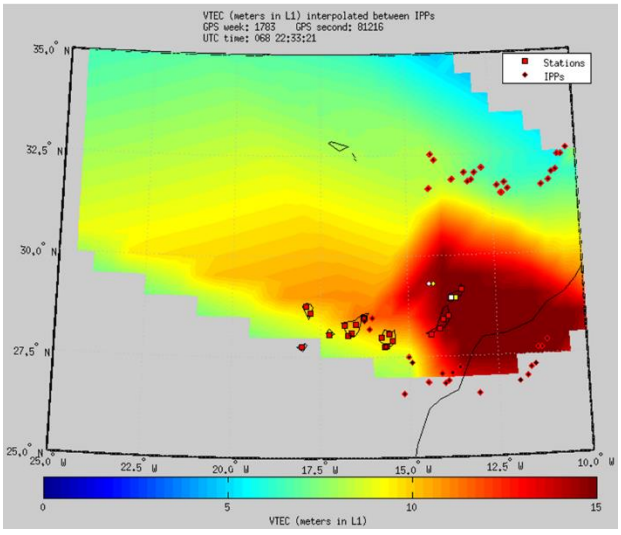

Figure 6-5. Gradient 7 VTEC map.

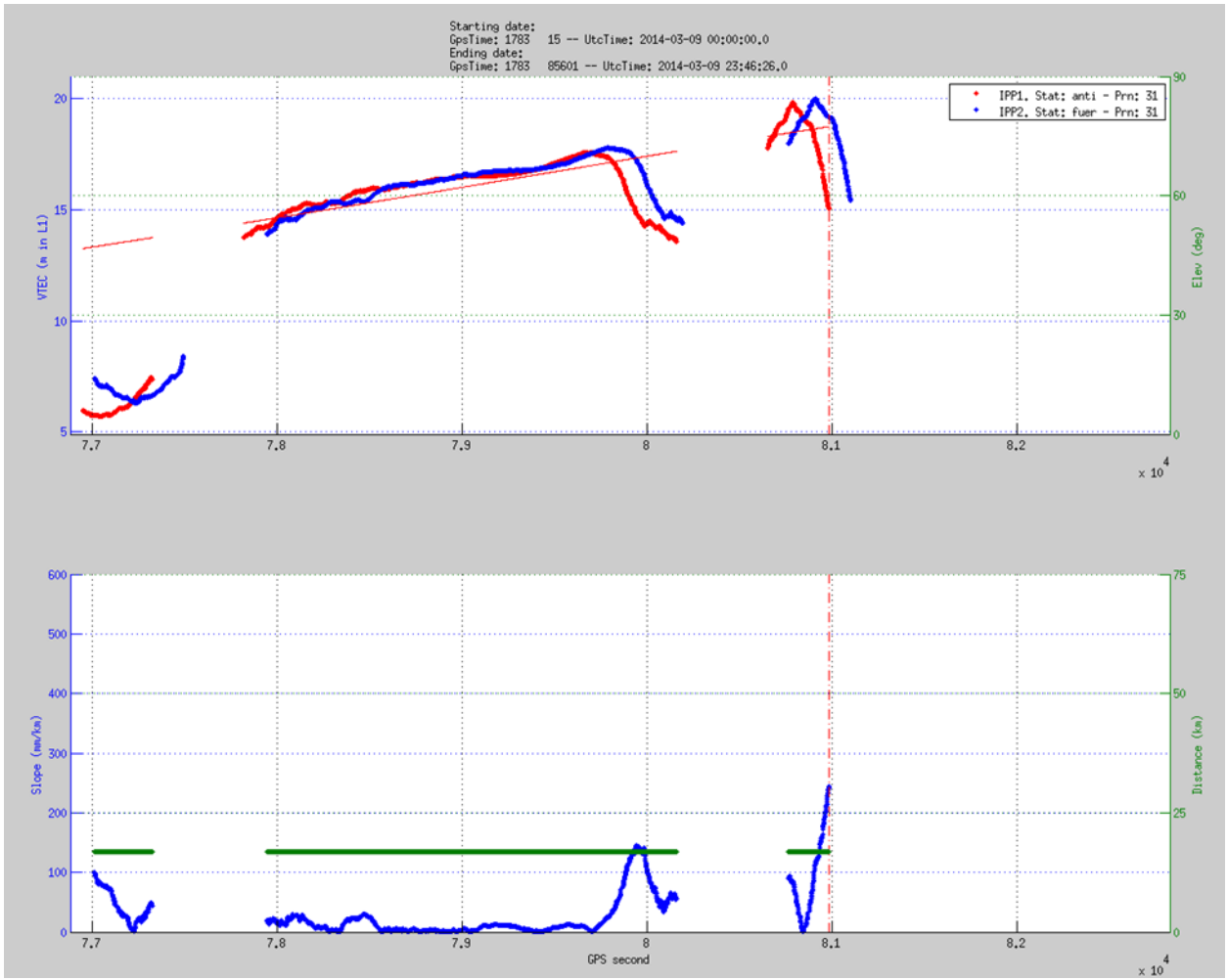

Figure 6-6. Gradient 2. VTEC and gradient.

6.3. PERIOD 56

Table below shows the largest gradients for this period.

Table 6-4 Period 56. Gradients

Gradient Id	Set	GPS Time	UTC Time	Station A	Station B	PRN	Elevation [º]	IPP Dist [km]	$Grad_{TRUE}$ VTEC [mm/km]	$Grad_{TRUE}$ STEC [mm/km]
~~31~~	~~1~~	~~90504~~	~~01h08:08~~	~~argu~~	~~mas1~~	~~12~~	~~27.5~~	~~4.5~~	~~*313~~	~~568.3~~
23	1	90934	01h15:28	snmg	tn03	12	30.8	10.6	212.2	360.4

Note. Considering that gradients 31 and 23 are obtained with the PRN 12, it would be expected to obtain similar gradients. However it is not the case, and gradient 31 is suspected to be over-estimated. For this reason, Gradient 31 is put on quarantine and not included in the ionosphere model.

Gradients detected in this period occurred around 1h (local time), during the night.

These gradients are due to enhance IEA, not bubbles. It is confirmed thanks to the temporal evolution of the ionospheric delay shown in §9.

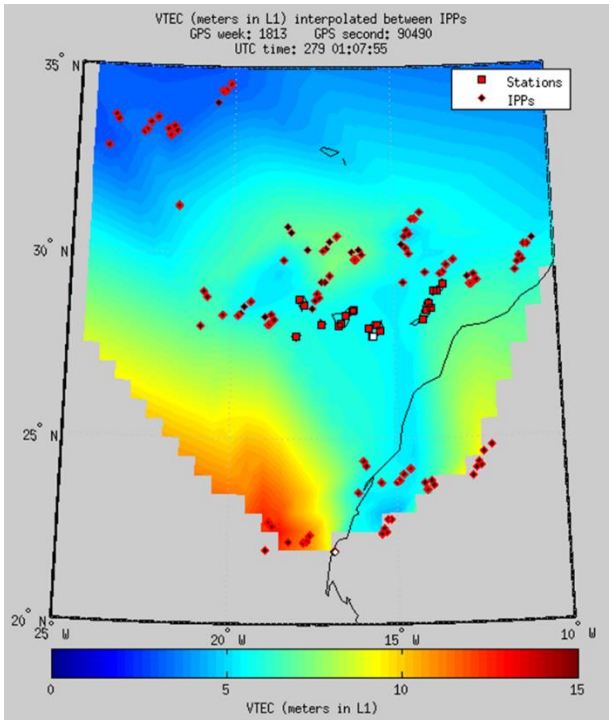

Figure 6-7. Gradient 31 VTEC map.

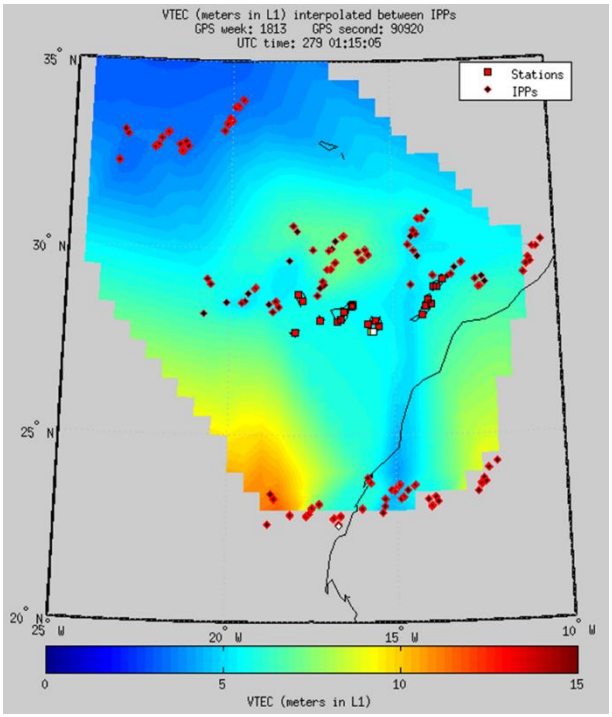

Figure 6-8. Gradient 23 VTEC map.

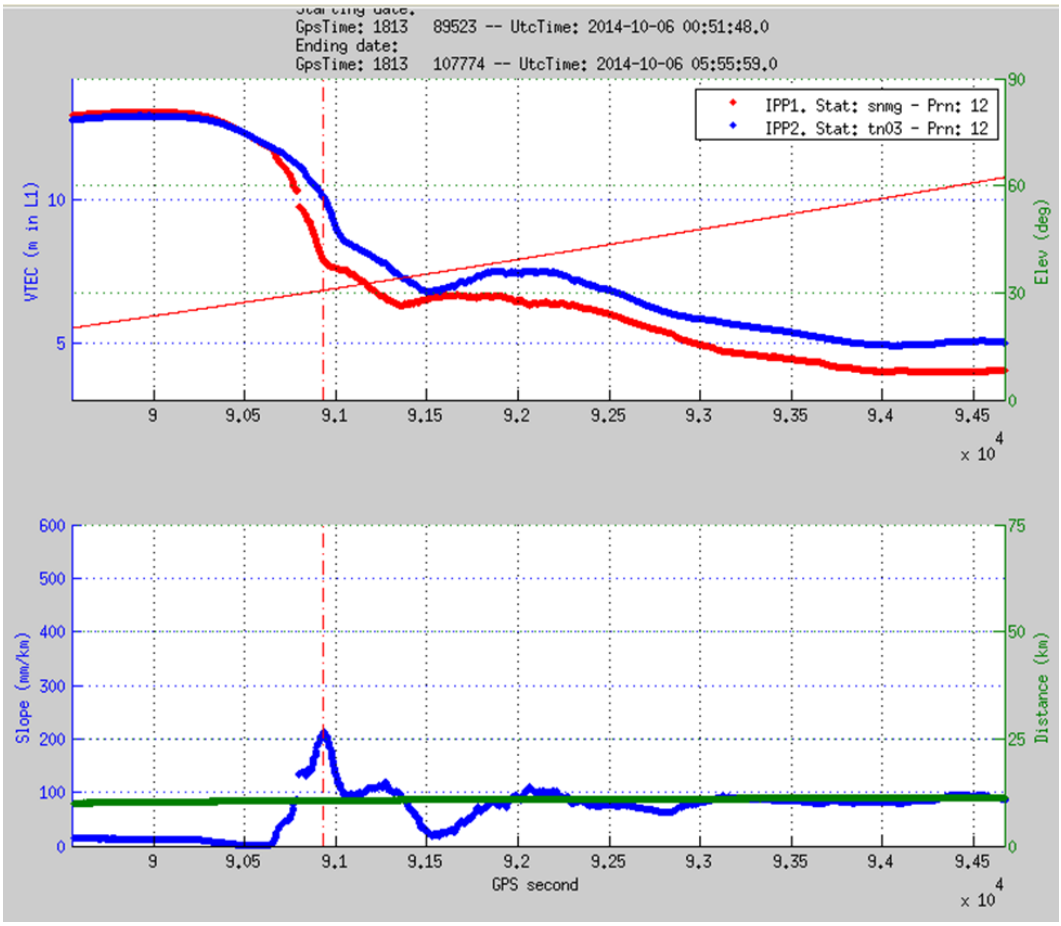

Figure 6-9. Gradient 23. VTEC and gradient.

6.4. PERIOD 51

Table below shows the largest gradients for this period.

Table 6-5 Period 51. Gradients

Gradient Id	Set	GPS Time	UTC Time	Station A	Station B	PRN	Elevation [°]	IPP Dist [km]	$Grad_{TRUE}$ VTEC [mm/km]	$Grad_{TRUE}$ STEC [mm/km]
93	1	602088	23h14:32	argu	mas1	2	62.7	4.6	*226	250.5
19	1	601309	23h01:33	alde	terr	6	46.2	23.6	220.4	290.4
21	1	601395	23h02:59	agui	argu	6	45.8	27	215.7	285.8

Gradients detected in this period occurred around 23h (local time), after sunset.

These gradients are due to enhance IEA, not bubbles. According to the temporal evolution of the ionospheric delay shown in §9. there are not any evidence of bubbles.

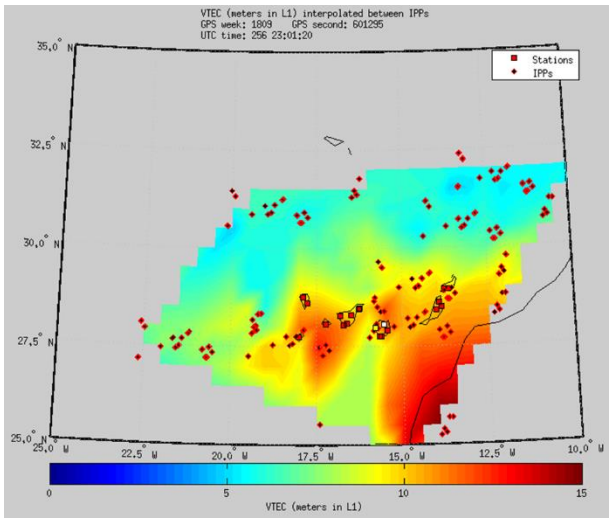

Figure 6-10. Gradient 19 VTEC map.

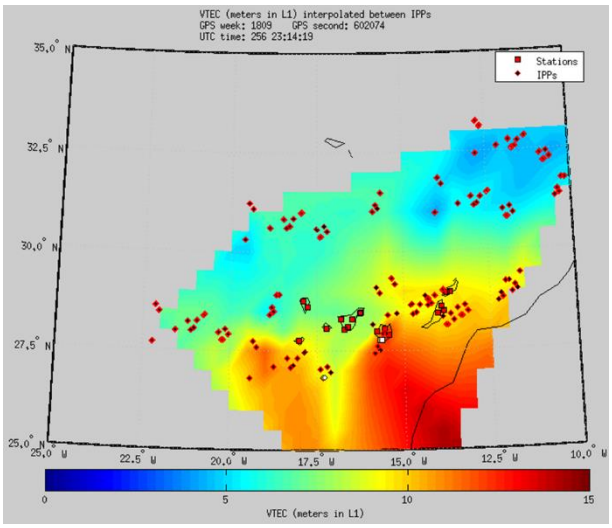

Figure 6-11. Gradient 93 VTEC map.

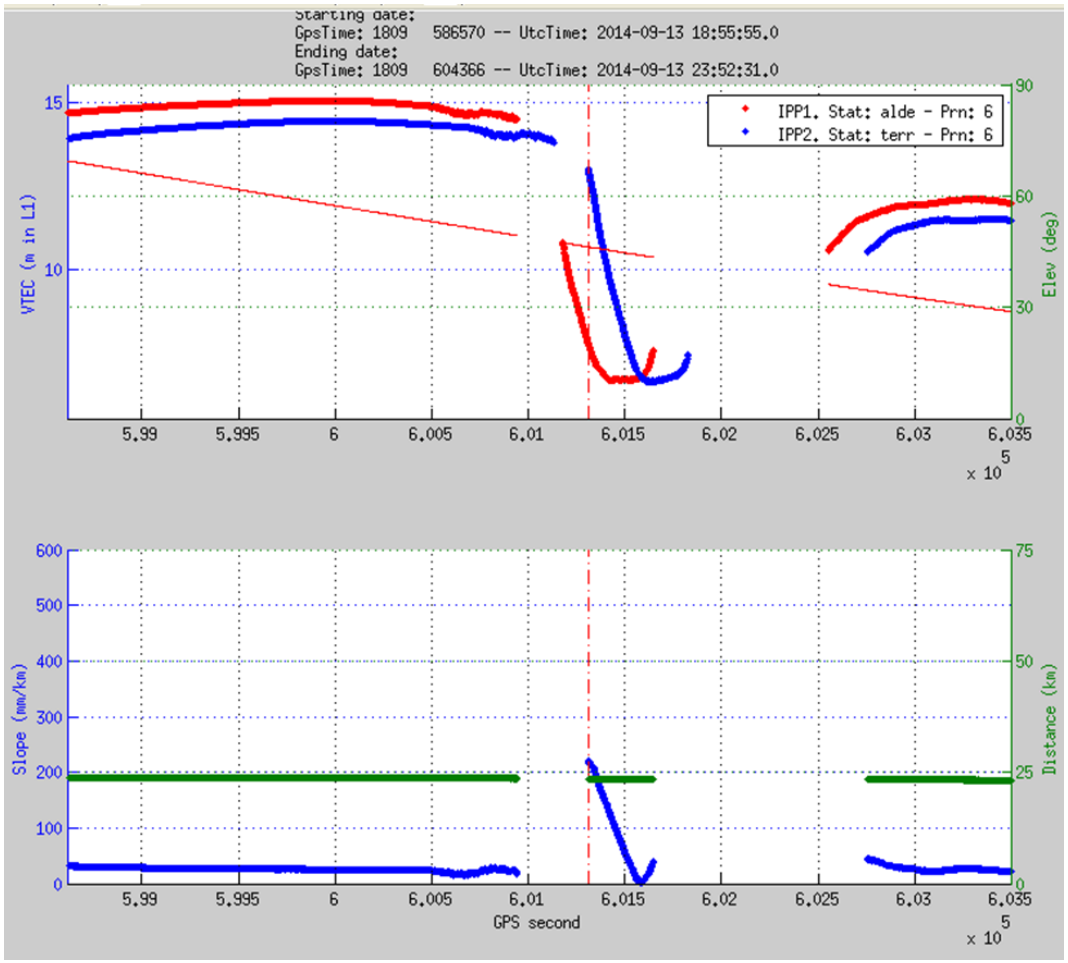

Figure 6-12. Gradient 19. VTEC and gradient.

6.5. PERIOD 34

Table below shows the largest gradients for this period.

Table 6-6 Period 34. Gradients

Gradient Id	Set	GPS Time	UTC Time	Station A	Station B	PRN	Elevation [º]	IPP Dist [km]	$Grad_{TRUE}$ VTEC [mm/km]	$Grad_{TRUE}$ STEC [mm/km]
13	1	251510	21h51:34	snmg	tn03	4	29.5	10.9	228.9	398.9
18	1	253242	22h20:26	tias	yaiz	2	43.2	10.4	222.7	306.1

Gradients detected in this period occurred around 22h (local time), after sunset.
These gradients are due to enhance IEA, not bubbles.

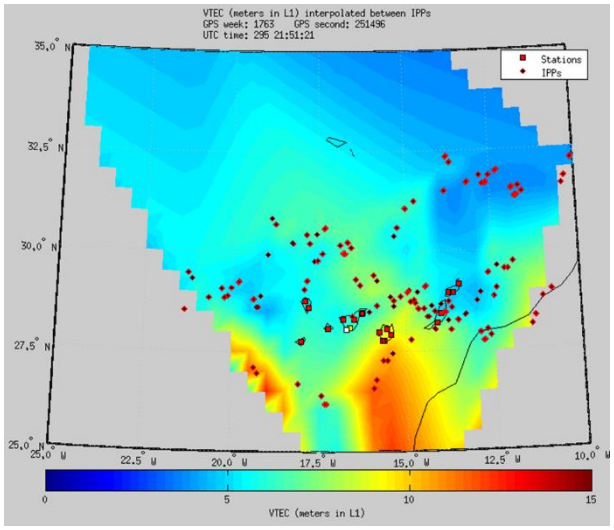

Figure 6-13. Gradient 13 VTEC map.

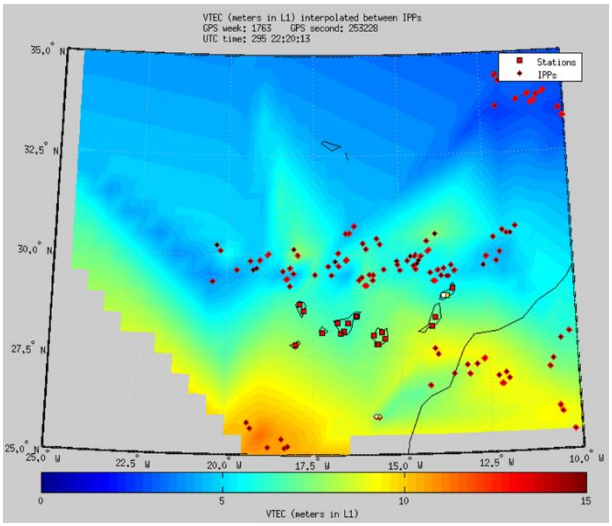

Figure 6-14. Gradient 18 VTEC map.

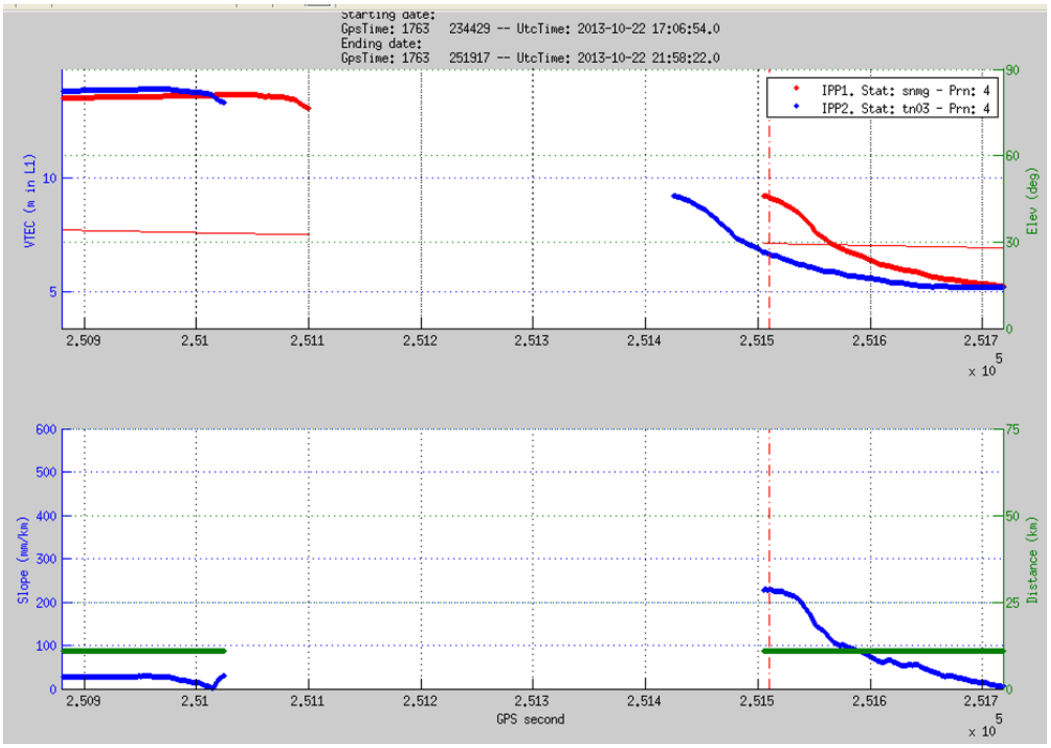

Figure 6-15. Gradient 13. VTEC and gradient.

6.6. PERIOD 55

Table below shows the largest gradients for this period.

Table 6-7 Period 55. Gradients

Gradient Id	Set	GPS Time	UTC Time	Station A	Station B	PRN	Elevation [º]	IPP Dist [km]	$Grad_{TRUE}$ VTEC [mm/km]	$Grad_{TRUE}$ STEC [mm/km]
16	1	4695	01h17:59	anti	fuer	12	29.0	15.6	225.7	397.3
44	1	4649	01h17:00	anti	oliv	12	28.7	18.3	192.9	341.7

Gradients detected in this period occurred around 01h (local time).
These gradients are due to enhance IEA, not bubbles.

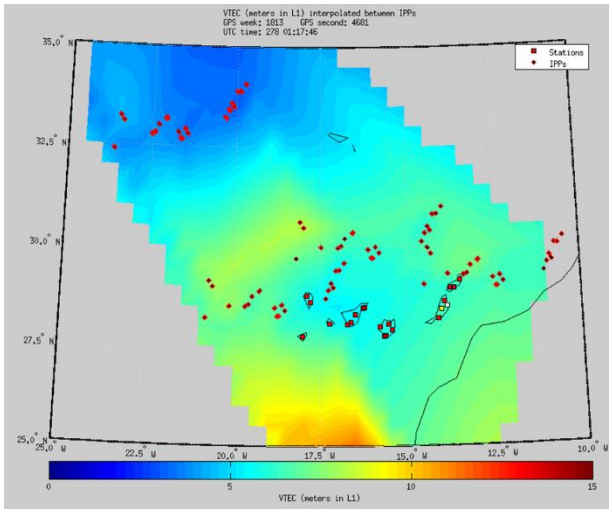

Figure 6-16. Gradient 16 VTEC map.

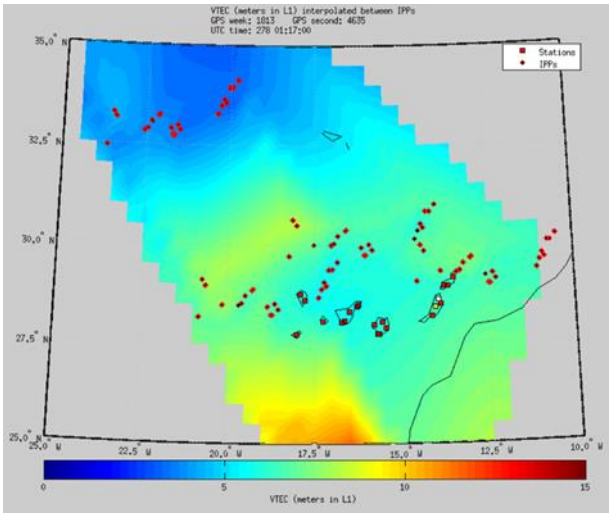

Figure 6-17. Gradient 44 VTEC map.

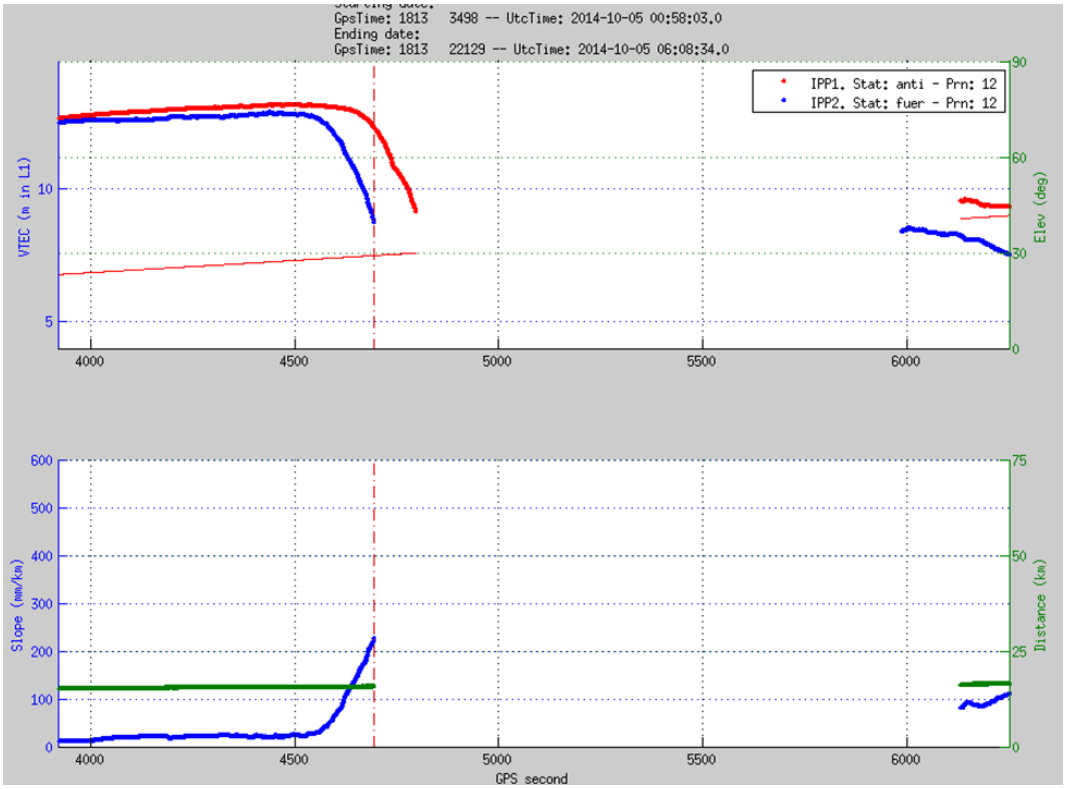

Figure 6-18. Gradient 16. VTEC and gradient.

7. CONCLUSIONS

Along this document the largest spatial gradients of ionospheric delay from 2009 to 2015 (SC 24) over Canary Islands are identified. The computation of gradients has been done using single-sv thanks to the high density of stations (cluster of Canary Islands).

After analysing the periods identified in SC 24, the largest gradients obtained are listed in Table 6-1 and further information and plots are included in §6.

7.1. GAST-C MODEL

For GBAS GAST-C stations there is an ionospheric threat model to define the spatial ionospheric gradients covered by the monitoring systems of the station. Any gradient not covered by the model will generate an integrity risks.

The threat model defines the maximum gradient, measured in slant (STEC), for the corresponding elevation of the IPPs.

The most significant gradients are displayed in Figure 7-1 and Figure 7-2 with respect to the ionospheric threat model for GBAS GAST-C stations (gradient in slant vs elevation).

The most significant (i.e. largest) gradients obtained at medium and high elevations, are covered by the ionospheric threat model of GBAS GAST-C station. Nevertheless, **gradients over the threshold have been confirmed** at low-mid-elevations, which potentially may generate integrity risks in GBAS GAST-C stations. Considering that SC#24 has been less active than previous, and that some gradients are not covered by the model, it is recommended to update the model increasing the maximum gradient.

These gradients, which are slightly above (<10 mm/km) the limits of the model at low-mid-elevation (~25º), are:

- Set 1. #7. Gradient 13. Period 34.
- Set 1. #9. Gradient 16. Period 55.
- Set 1. #16. Gradient 25. Period 53.
- Set 2. #12. Gradient 34. Period 38.

Note. An uncertainty of 0.1m in the estimation of the station hardware bias, would provoke an uncertainty of 10mm/km in the gradient estimated, if the baseline distance between the pair of stations were 20km.

The remaining gradients are below the limit, maintaining a safe-gap (>25 mm/km) with respect to the limit. Based on the definition of the model, it should be confirmed either:

a. these events just above the limit are acceptable because they are unlikely (4 events during the whole solar-cycle), or
b. the model should be revised to increase the limits at low-mid-elevations.

Note. In the model (Figure 7-1 and Figure 7-2), gradients in slant (STEC) are plotted, instead of vertical gradients (VTEC) displayed in tables and figures of §6. .

In addition, the model includes the following statistics: maximum, minimum and mean gradient of each event. These statistics are computed within 50 epochs (seconds) around the maximum gradient.

Finally, it is observed that all the highest gradients found in the Canary Islands have been generated by the enhanced activity of the daily build-up of the ionospheric equatorial anomaly (IEA) (i.e. no front due to ionospheric storms has been found). Further information in Annex II §9.

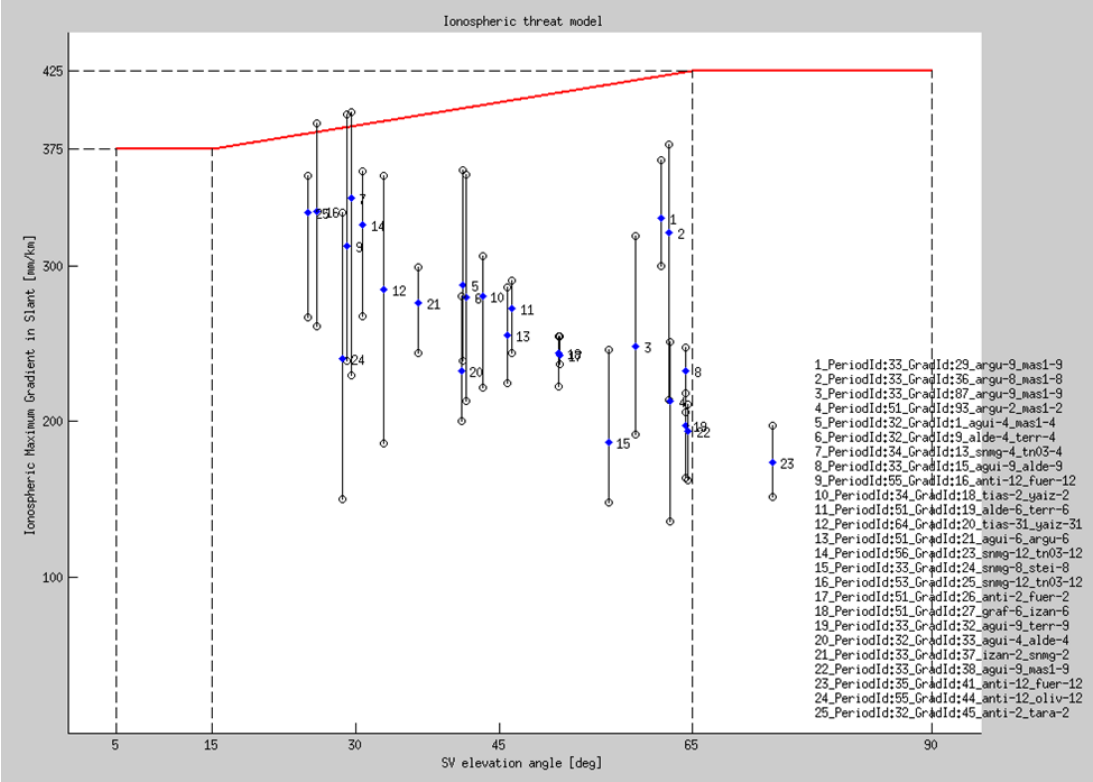

Figure 7-1. Ionospheric threat model in Canary Islands. Gradients in STEC (slant). Set 1.

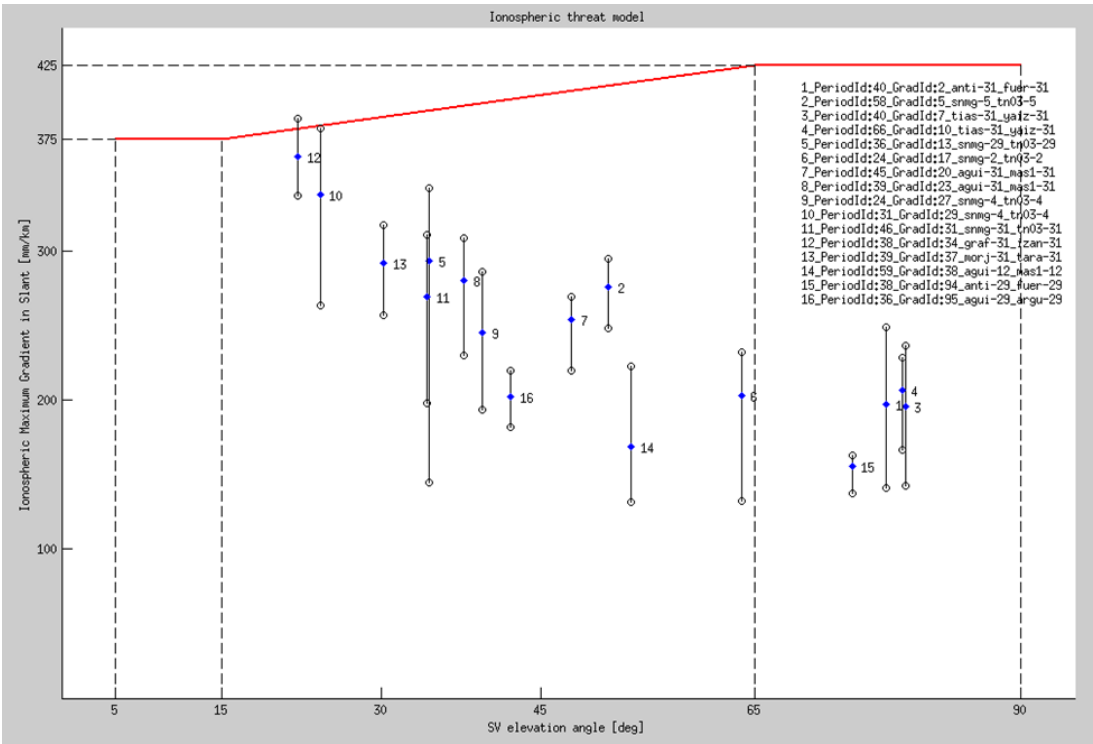

Figure 7-2. Ionospheric threat model in Canary Islands. Gradients in STEC (slant). Set 2.

7.2. GAST-D MODEL

For GBAS GAST-D stations there is an updated ionospheric threat model to define the spatial ionospheric gradients covered by the monitoring systems of the station. Any gradient not covered by the model will generate an integrity risks.

The model defined in GAST-D SARPS baseline below is shown below:

Table D-5A

Propagation Speed (v)	**Upper Bound on Gradient Slope (g)**
v < 750 m/s	500 mm/km
750 ≤ v < 1500 m/s	100 mm/km

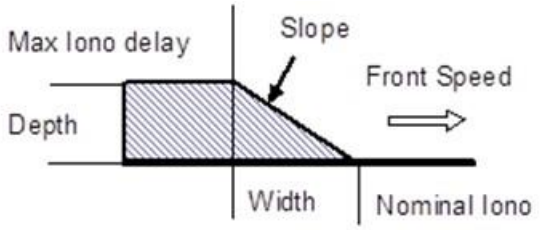

Figure D-1A: Moving Wedge Ionospheric Anomaly Model

Note. The threat model defines the maximum gradient, measured in slant (STEC), for the corresponding propagation speed of the front. Elevation of the IPPs is not included in this model. The maximum value of the ionospheric error is 50m, computed as:

$$D = g * w$$

where:

D is the depth (ionospheric error) [m]

g is the slope (slant gradient) [mm/km]

w is the width of the front [km]

Gradients whose depth is greater than 50m are not covered by the model.

In the results obtained in this document have not been estimated neither the propagation speed (v) nor the width (w) of the front, because they were not the scope of the analyses.

8. ANNEX I: MANUAL CORRECTION

This annex describes how some gradients have been manually corrected to obtain the true gradient. This correction is needed in some cases where the distance between IPPs is very small, where small errors during the estimation of the stations' hardware bias might provoke large errors in the estimation of the gradients.

8.1. GRADIENT 29

Comparing the VTEC values of argu with near stations (less than 50km), the arc generating the largest gradient is slightly above the VTEC values of the near stations (~0.5m), making the gradient being over-estimated.

$$Grad_{TRUE} = Grad - {}^{\Delta VTEC}/_{IPPDist} = 439 - {}^{500}/_{4.6} = 330\ mm/km$$

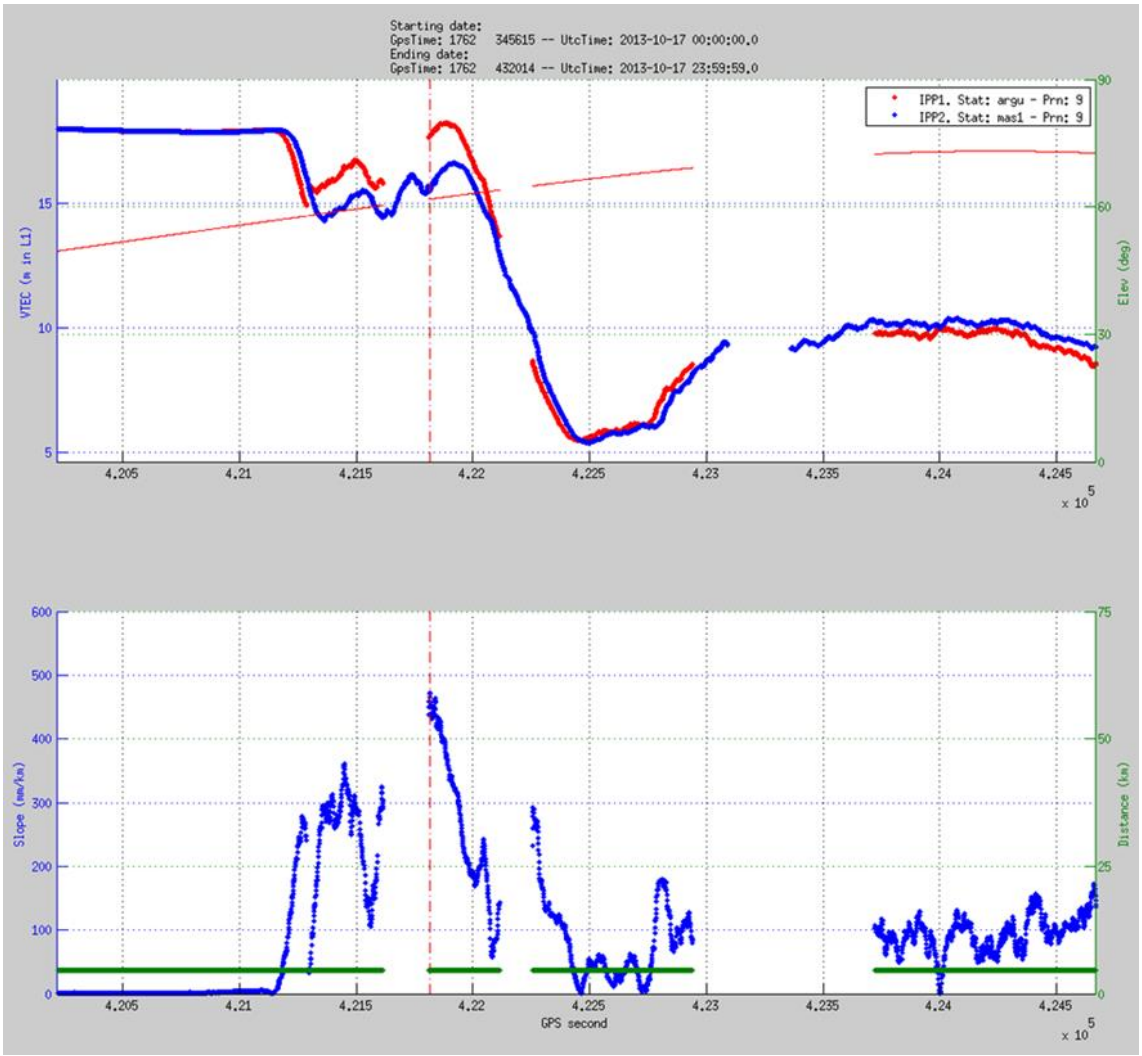

Figure 8-1. Gradient 29. VTEC and gradient.

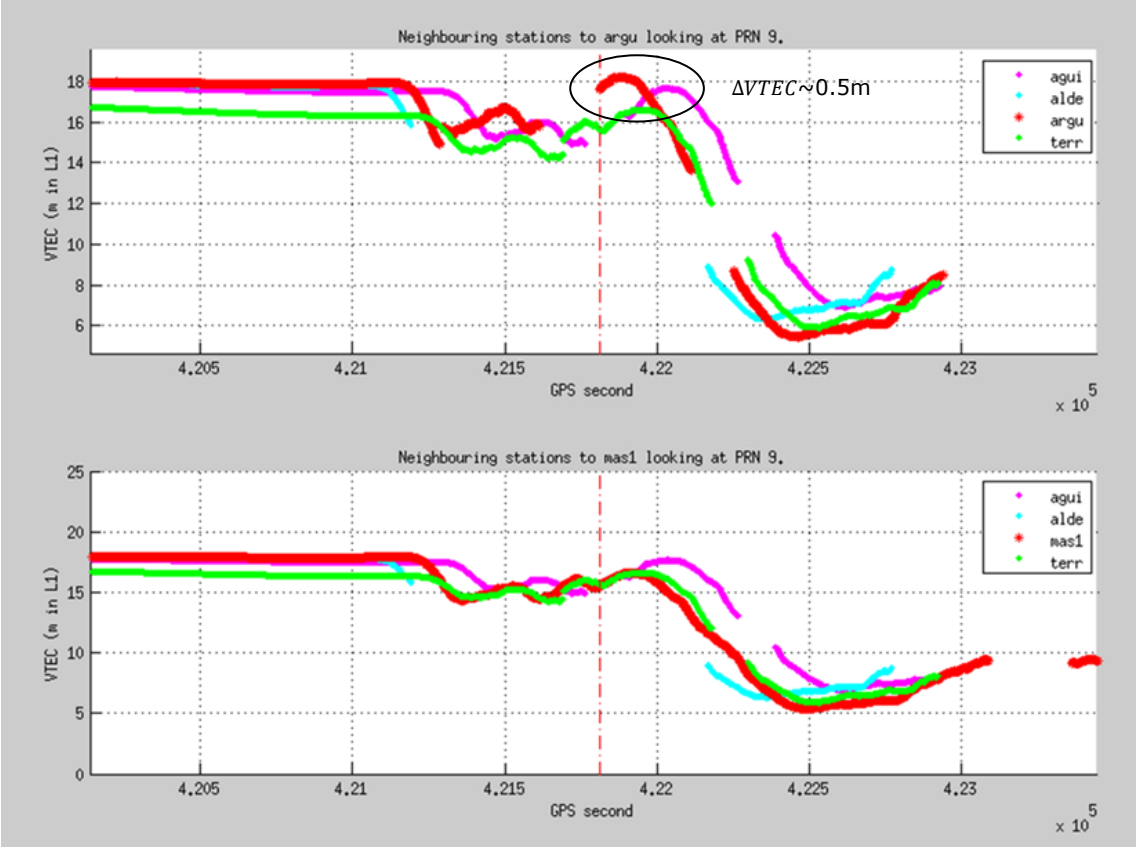

Figure 8-2. Gradient 29. VTEC of near stations.

8.2. GRADIENT 36

Comparing the VTEC values of argu with near stations (less than 50km), the arc generating the largest gradient is slightly above the VTEC values of the near stations (~1.2m), making the gradient being over-estimated.

$Grad_{TRUE} = Grad - {}^{\Delta VTEC}/_{IPPDist} = 602 - {}^{1200}/_{4.6} = 341\ mm/km$

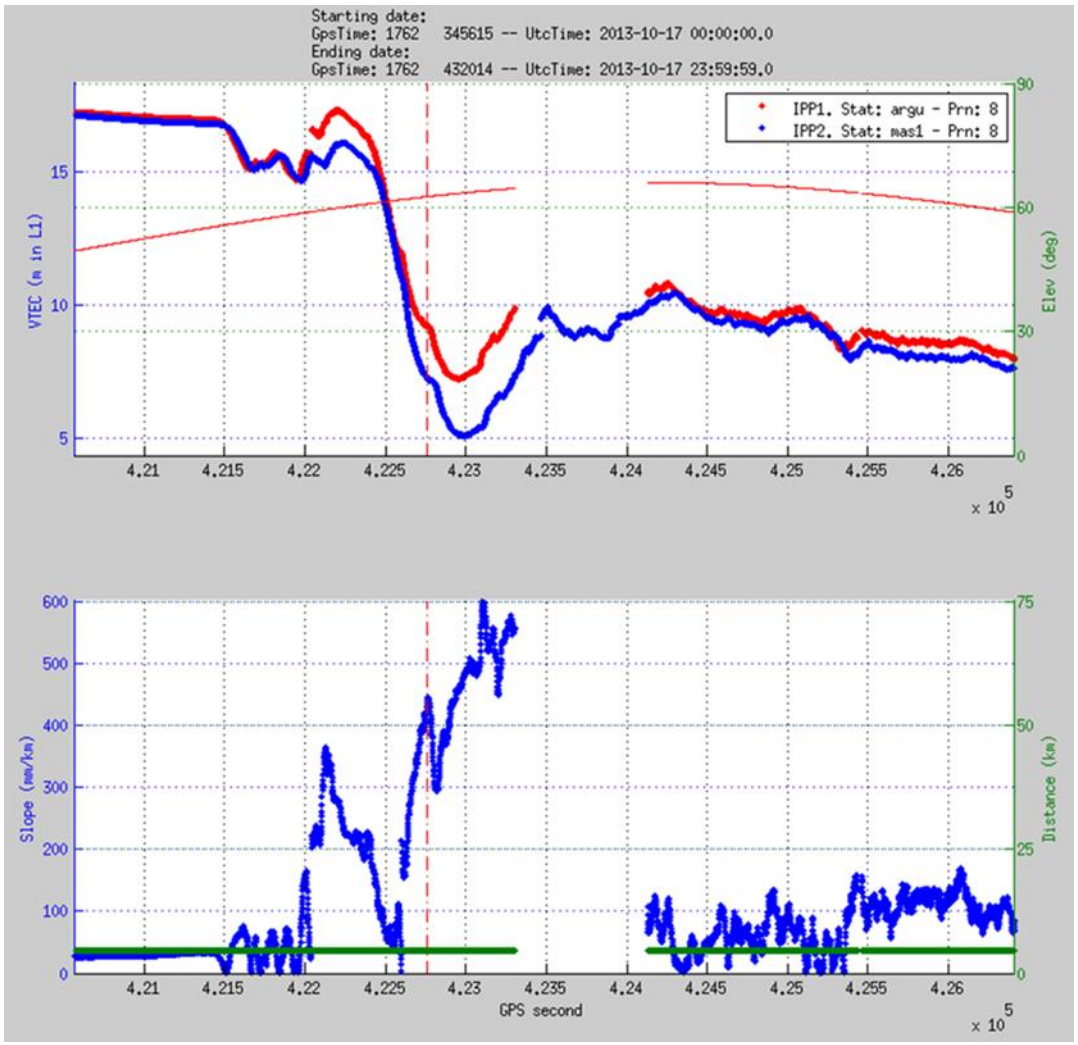

Figure 8-3. Gradient 36. VTEC and gradient.

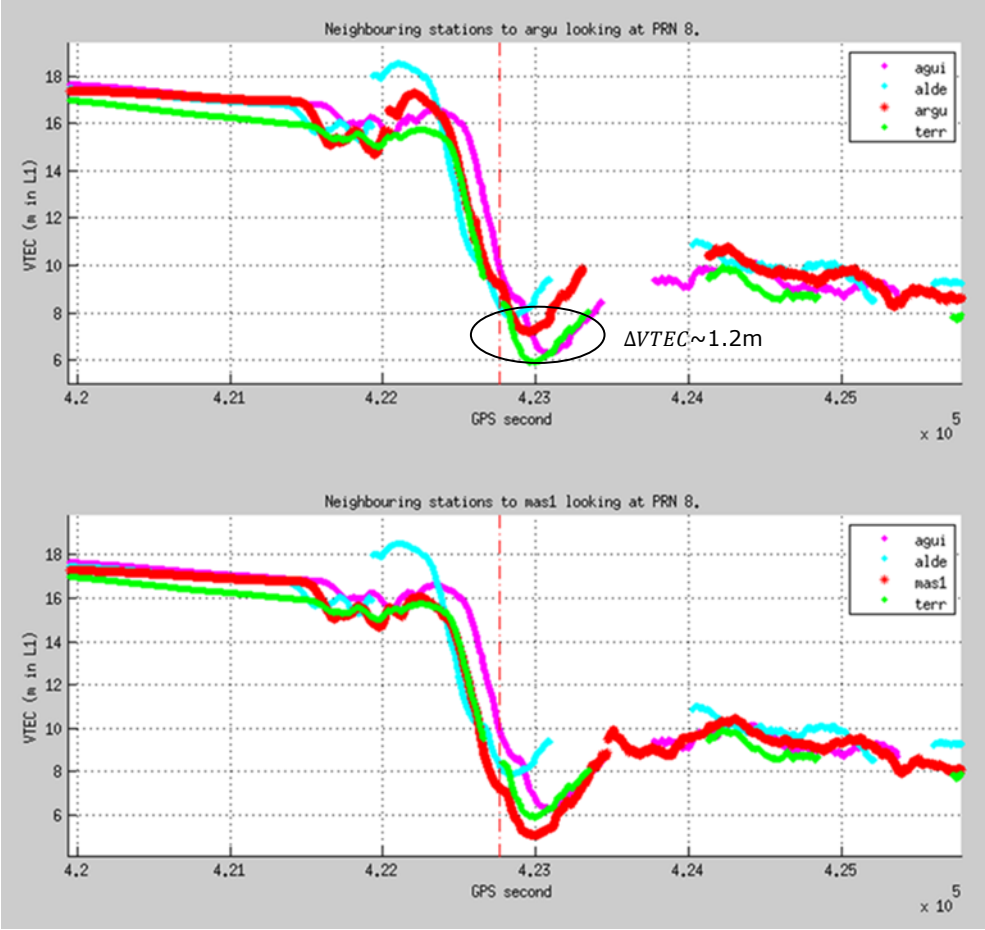

Figure 8-4. Gradient 36. VTEC of near stations.

8.3. GRADIENT 87

Comparing the VTEC values of argu with near stations (less than 50km), the arc generating the largest gradient is slightly above the VTEC values of the near stations (~0.5m), making the gradient being over-estimated.

$Grad_{TRUE} = Grad - {}^{\Delta VTEC}/_{IPPDist} = 360 - {}^{500}/_{4.6} = 251\, mm/km$

Nevertheless, the gradient of 279mm/km occurring before (see figure below) is valid. So this value is used for gradient 87.

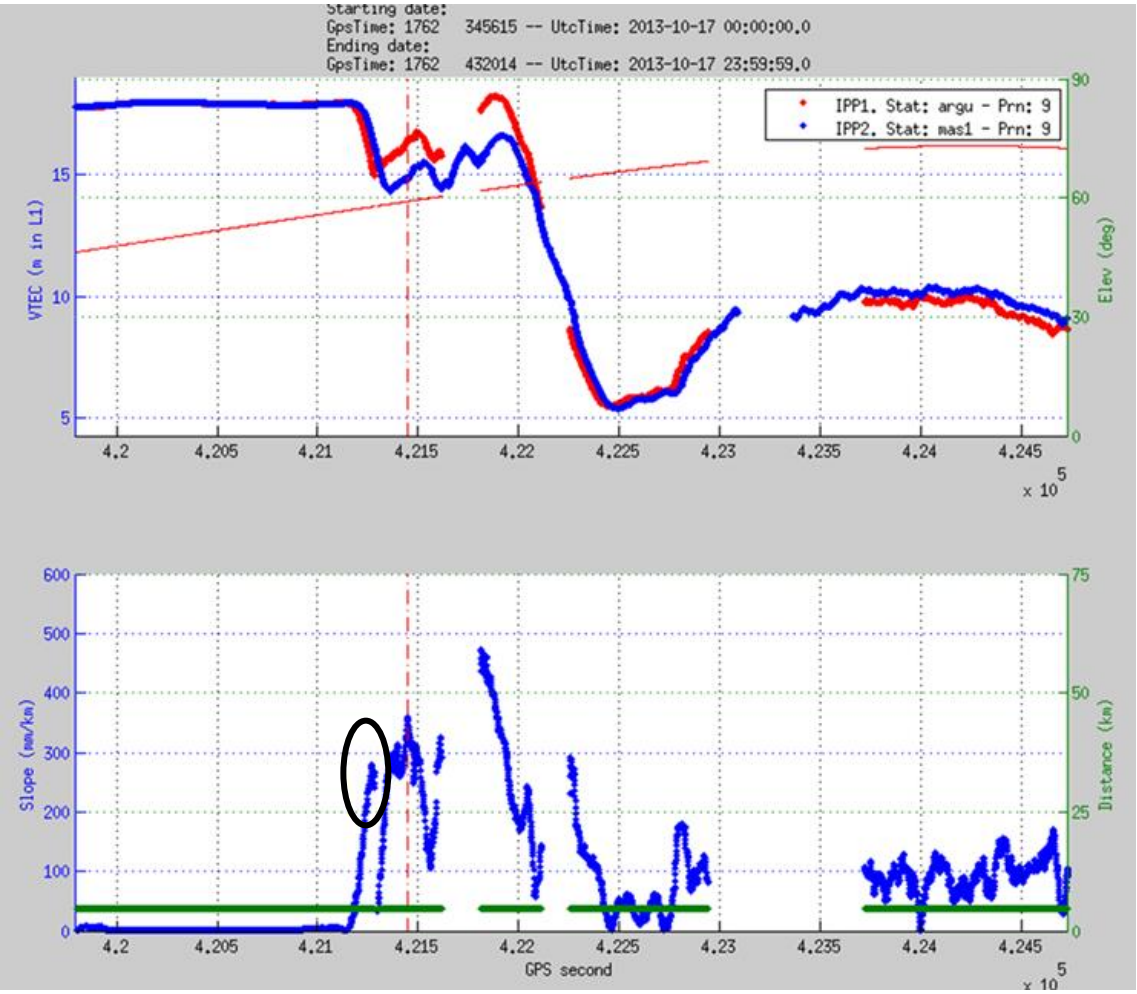

Figure 8-5. Gradient 87. VTEC and gradient.

8.4. GRADIENT 31

Observing the VTEC values of argu and mas1 at the beginning of the arc, there is an offset which should be close to 0, as in the near stations (less than 50km). For this reason, the almost constant gradient at the beginning of the arc should be close to 0.0 instead of 148mm/km.

In order to obtain the true gradient, the gradient due to the offset has to be removed.

$Grad_{TRUE} = Grad - Grad_{offset} = 461 - 148 = 313\ mm/km$

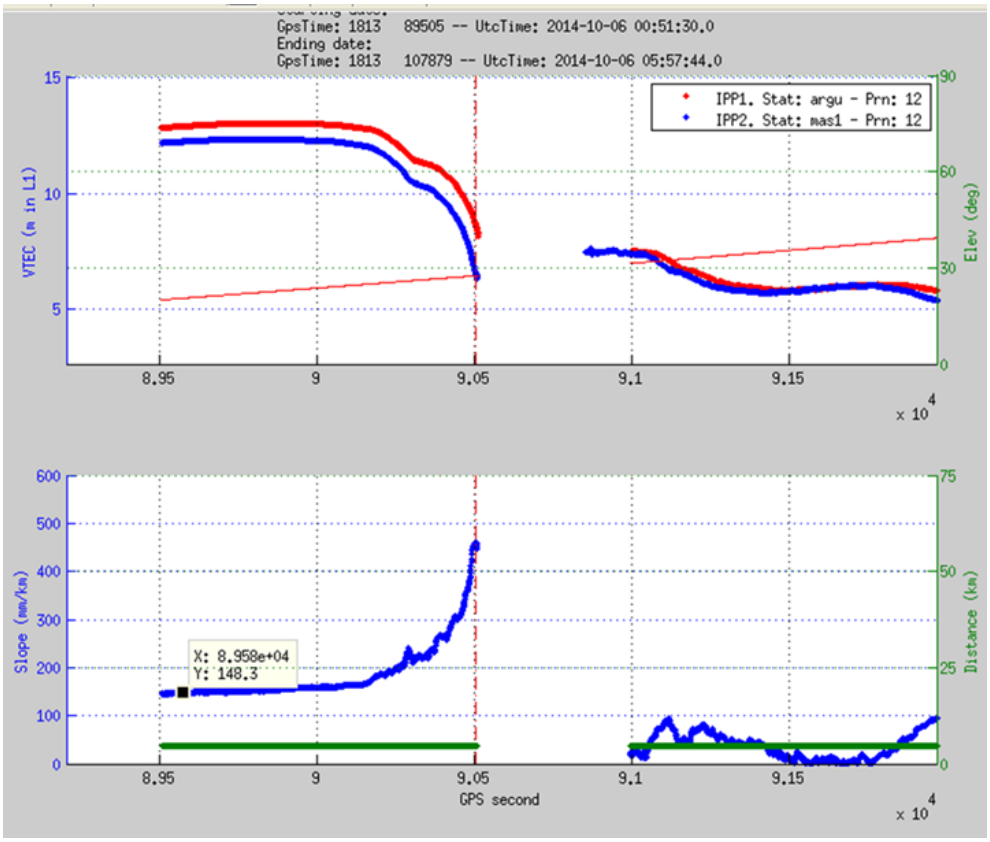

Figure 8-6. Gradient 31. VTEC and gradient.

8.5. GRADIENT 93

Comparing the VTEC values of argu with near stations (less than 50km), the arc generating the largest gradient is slightly above the VTEC values of the near stations (~0.6m), making the gradient being over-estimated.

$$Grad_{TRUE} = Grad - {}^{\Delta VTEC}/_{IPPDist} = 357 - {}^{600}/_{4.6} = 226\ mm/km$$

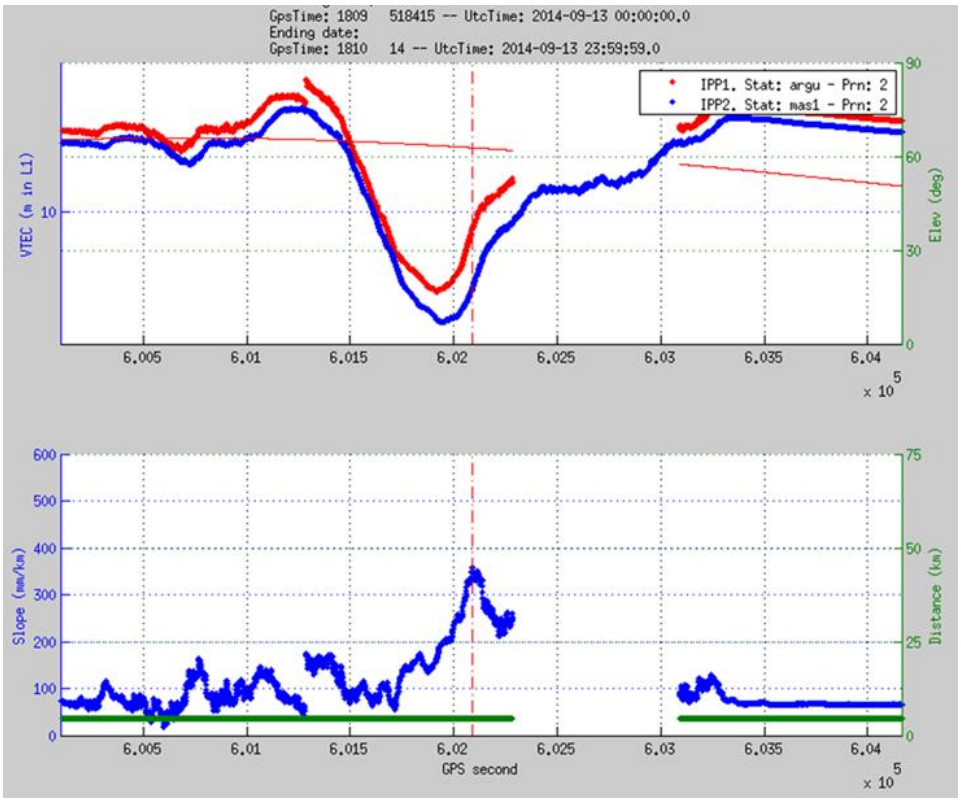

Figure 8-7. Gradient 93. VTEC and gradient.

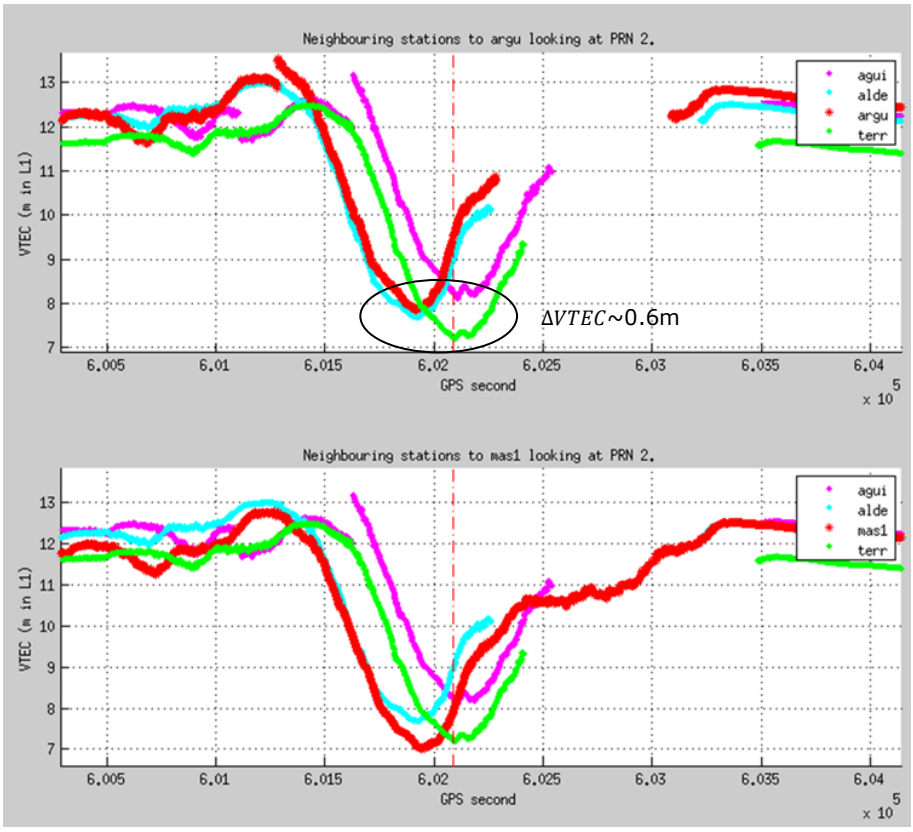

Figure 8-8. Gradient 31. VTEC of near stations.

8.6. GRADIENT 1

Observing the VTEC values of agui, there is a jump in the second arc (mainly due to the leverage using with P2). For this reason, gradients on the second arc should be rejected.

Nevertheless the VTEC estimation in first arc is valid for both IPPs, and the gradient is therefore reliable.

$Grad_{TRUE} = 255\ mm/km$

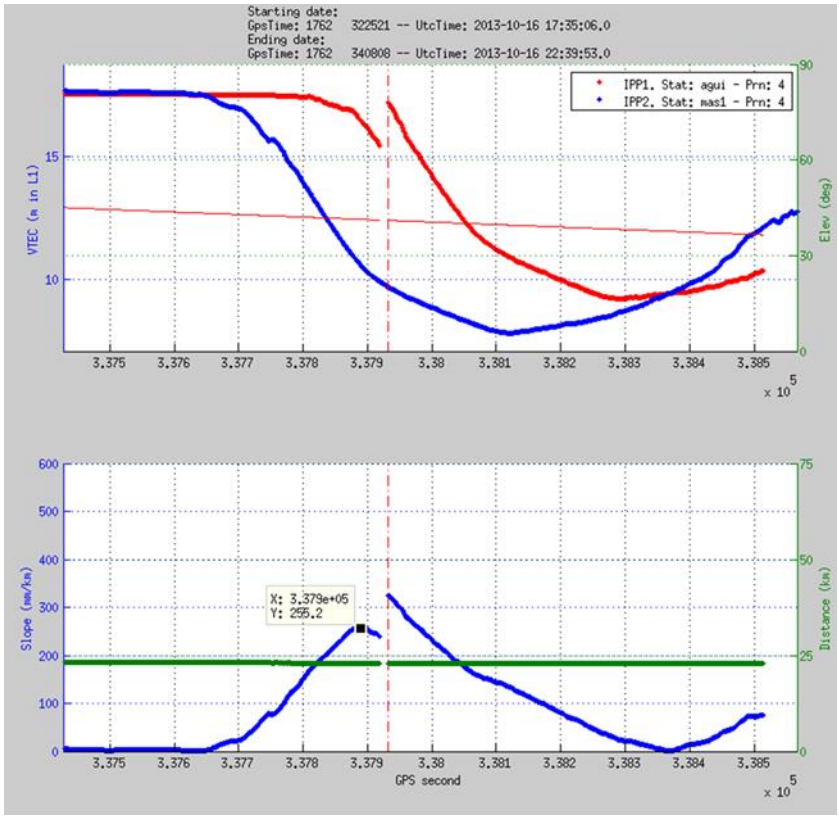

Figure 8-9. Gradient 1. VTEC and gradient.

9. ANNEX II: IONOSPHERIC EVENTS

This annex describes that the types of ionospheric events detected in this analyses belong to the enhanced activity of the ionospheric equatorial anomaly (IEA).

This annex includes 5 videos displaying the VTEC on a map along the day of each period. These videos are created taking a picture of the ionosphere every 3 minutes.

Table 9-1. Videos with ionosphere evolution.

Filename	Period
VtecMovPeriod_33_compress.avi	33
VtecMovPeriod_51_compress.avi	51
VtecMovPeriod_56_compress.avi	56
VtecMovPeriod_58_compress.avi	58
VtecMovPeriod_66_compress.avi	66

Thanks to the behaviour of the ionosphere along time observed in these videos, it is confirmed the origin of the gradients is the IEA.

Period 33.

Some screenshots of VTEC maps are shown below to confirm the type of event.

10h00 – Low activity of the ionosphere	15h00 – Increasing activity of the ionosphere during daylight.
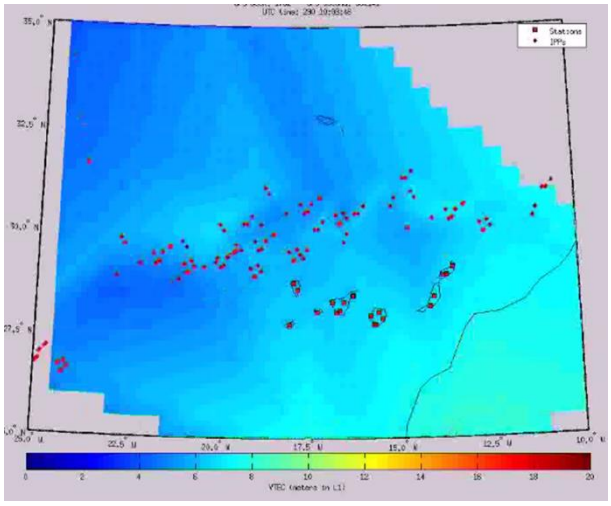	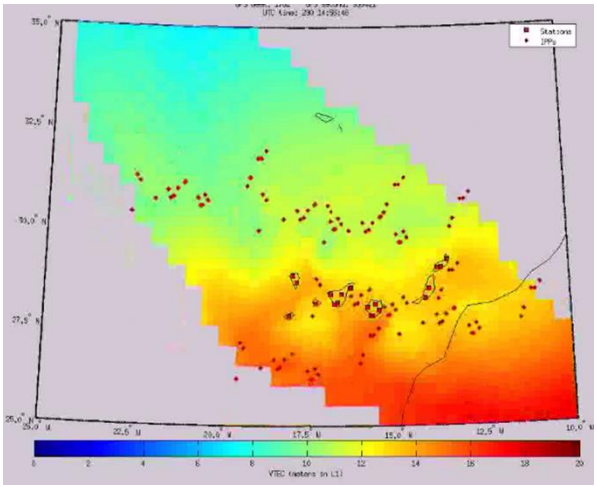

20h30 – High activity of the ionosphere during sunset.	23h00 – Decreasing activity of the ionosphere after sunset
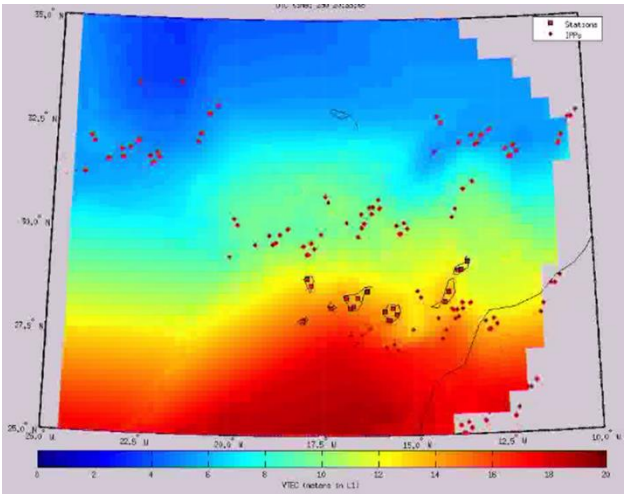	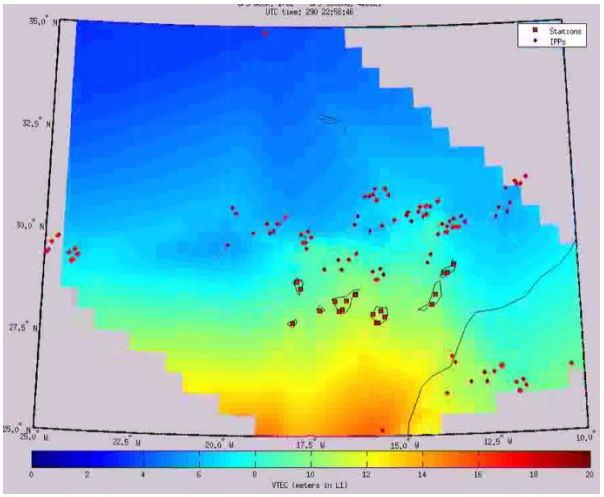

END OF DOCUMENT

